Chemical Geology 285 (2011) 97–114

Contents lists available at ScienceDirect

Chemical Geology

journal homepage: www.elsevier.com/locate/chemgeo

Geochemistry and Sr–Nd–Pb–Hf isotopes of the Mesozoic Dadian alkaline intrusive complex in the Sulu orogenic belt, eastern China: Implications for crust–mantle interaction

Ting-Guang Lan [a], Hong-Rui Fan [a,*], M. Santosh [b], Fang-Fang Hu [a], Kui-Feng Yang [a], Yue-Heng Yang [a], Yongsheng Liu [c]

[a] Key Laboratory of Mineral Resources, Institute of Geology and Geophysics, Chinese Academy of Sciences, Beijing 100029, China
[b] Division of Interdsciplinary Science, Faculty of Science, Kochi University, Kochi 780-8520, Japan
[c] State Key Laboratory of Geological Processes and Mineral Resources, China University of Geosciences, Wuhan 430074, China

ARTICLE INFO

Article history:
Received 9 November 2010
Received in revised form 11 March 2011
Accepted 15 March 2011
Available online 25 March 2011

Editor: U. Brand

Keywords:
Alkaline intrusive complex
Enriched lithospheric mantle
Crust–mantle interaction
Syenite
Dadian
Sulu orogenic belt

ABSTRACT

The Dadian alkaline intrusive complex is located within the Sulu orogenic belt, and includes hornblende syenite, syenite, quartz syenite and syenite porphyry. All the rocks from the complex show high SiO_2, K_2O+Na_2O and LREE and low CaO, FeO^T, MgO and HFSE (Nb, Ta, P, Ti) concentrations. The Sr, Nd, and Hf isotopic compositions ($(^{87}Sr/^{86}Sr)_i=0.708505–0.70876$, $\varepsilon_{Nd}(t)=-16.5$ to -17.9, $\varepsilon_{Hf}(t)=-21.5$ to -16.4) of the rocks fall within the compositional field of mafic dykes occurring nearby, suggesting that the Dadian alkaline complex was mainly derived from an enriched lithospheric mantle. The initial Pb compositions ($(^{206}Pb/^{204}Pb)_i=16.706–16.779$, $(^{207}Pb/^{204}Pb)_i=15.427–15.450$, $(^{208}Pb/^{204}Pb)_i=37.266–37.352$) of the Dadian rocks are lower than those of the Yangtze lithospheric mantle, albeit similar to that reported from beneath the North China Craton, implying that the mantle source of the Dadian alkaline complex most likely belong to the North China Craton. The relatively high SiO_2 and HREE contents and low Nb/Ta ratios as well as strongly negative Eu and Sr anomalies of some of the rocks from the Dadian complex suggest that crustal material was also involved in the formation of this complex and that the crustal component was probably derived through partial melting at low pressure. The high crystallization temperatures revealed by zircon saturation thermometry and low pressures suggested by Al-in-hornblende barometry indicate that the Dadian alkaline complex crystallized at high temperature and intruded into shallow crustal level. This intrusive complex does not show any relationship with post-orogenic process in the region, and its petrogenesis is inferred to be associated with the Paleo-Pacific subduction tectonics.

1. Introduction

Mesozoic igneous rocks in the Sulu orogenic belt of eastern China include late Triassic alkaline intrusive complexes, late Jurassic granitoid rocks and early Cretaceous mafic to acidic magmatic rocks (Guo et al., 2005; Zhao and Zheng, 2009). The late Triassic alkaline intrusive complexes and the late Jurassic granitoid rocks are related to collision or post-collision process between the North China Craton (NCC) and the Yangtze Craton (YC) (Chen et al., 2003b; Gao et al., 2004; Zhang et al., 2004; Guo et al., 2005; Yang et al., 2005b; Xie et al., 2006b; Siebel et al., 2009; Zeng et al., 2009; Zhao and Zheng, 2009). The petrogenesis of the widespread early Cretaceous magmatic rocks consisting of minor pyroxenites/gabbros and mafic dykes and abundant granites, syenites, monzonites and volcanic rocks (Zhou et al., 2003b; Wang et al., 2009a; Zhao and Zheng, 2009) remains equivocal, particularly with regard to the geodynamic setting and source material. Some workers have correlated these rocks with post-collisional processes (Li et al., 2002; Guo et al., 2006; Xie et al., 2006a; Xu et al., 2007; Zhao et al., 2007), whereas others consider that they are the products of lithosphere thinning of eastern China (Guo et al., 2005; Yang et al., 2005c). The lithospheres of both NCC and YC have been proposed as potential magma sources.

Most of the early Cretaceous intermediate to acidic intrusive rocks in the Sulu orogenic belt are enriched in K_2O+Na_2O. The syenitic rocks fall in the alkaline field and granites are generally A-type (Wang et al., 1995; Zhao et al., 1997; Wei et al., 2001; Liu et al., 2008a; Wang et al., 2009b). Alkaline rocks and A-type granites are usually generated in post-collision extensional settings (Nédélec et al., 1995; Bonin et al., 1998; Hadj-Kaddour et al., 1998; Liégeois et al., 1998; Yang et al., 2005b; Oyhantçabal et al., 2007), intra-plate rifts or deep faults (Melluso et al., 2002; Burke et al., 2003; Peccerillo et al., 2003; Ridolfi et al., 2006; Upadhyay et al., 2006; Jung et al., 2007; Kaymakci, et al., 2007; Shellnutt and Zhou, 2008), or by mantle plumes (Mchone,

* Corresponding author. Tel.: +86 10 82998218; fax: +86 10 62010846.
E-mail address: fanhr@mail.igcas.ac.cn (H.-R. Fan).

0009-2541/$ – see front matter © 2011 Elsevier B.V. All rights reserved.
doi:10.1016/j.chemgeo.2011.03.013

1996; Karmalkar et al., 2005; Muñoz et al., 2005; Srivastava et al., 2005). These rocks thus offer important information on the crust–mantle interaction and evolution of continental crust (Yang et al., 2007 and references therein).

The Dadian complex is the largest alkaline intrusive complex in the Sulu orogenic belt. In this paper, we report the geochronological, petrological and geochemical data on this complex, with an aim to constrain its petrogenesis and tectonic setting within the Sulu orogenic belt.

2. Geological background

The Sulu belt, the eastern part of the Dabie–Sulu Orogenic belt, formed during the Triassic collision between the North China and Yangtze Cratons (Fig. 1a; Zheng, 2008). The major components of the Sulu belt include Paleoproterozoic metamorphic rocks (Wang et al., 2004), Neoproterozoic granites and granitic gneisses (Zhou et al., 2003a; Wang et al., 2004; Huang et al., 2006; Xue et al., 2006a,b; Li et al., 2007b), Triassic ultrahigh- to high-pressure metamorphic rocks (Katsube et al., 2009; Li et al., 2009; Zhang et al., 2009b) and alkaline rocks, as well as late Jurassic granitoid rocks and early Cretaceous mafic to acidic magmatic rocks (Fig. 1b). The Dabie–Sulu orogenic belt has been in focus for evaluating the exhumation mechanism of subducted continental crust, orogenic evolution and crust–mantle interaction. The belt has also attracted considerable attention with regard to the early Cretaceous magmatic activity, and the question whether the magmatism was controlled by post-collisional processes or not.

The Dadian alkaline intrusive complex is located within the Dadian region of Junan county in the Sulu orogenic belt and is exposed over an area of 550 km^2 (Liu et al., 2008a). Quartz monzonite, hornblende syenite, syenite, quartz syenite, syenite porphyry and alkali-feldspar granite are the major components of the complex (Zhou et al., 2003b). This work mainly focuses on the alkaline rocks which include hornblende syenite, syenite, quartz syenite and syenite porphyry (Fig. 2).

3. Petrography

3.1. Hornblende syenite

The hornblende syenite is grayish white and consists typically of feldspar and hornblende with subordinate quartz and biotite and accessory titanite, apatite, zircon and magnetite. The subhedral–anhedral feldspars (90–95 vol.%) are perthite, albite, orthoclase and oligoclase (0.2–4 mm). The columnar or irregular hornblende is magnesiohornblende (1–5 vol.%, 0.5–1 mm). Quartz (<1 vol.%, <1 mm) is irregular. The subhedral–anhedral biotite (~1 vol.%, 0.5–

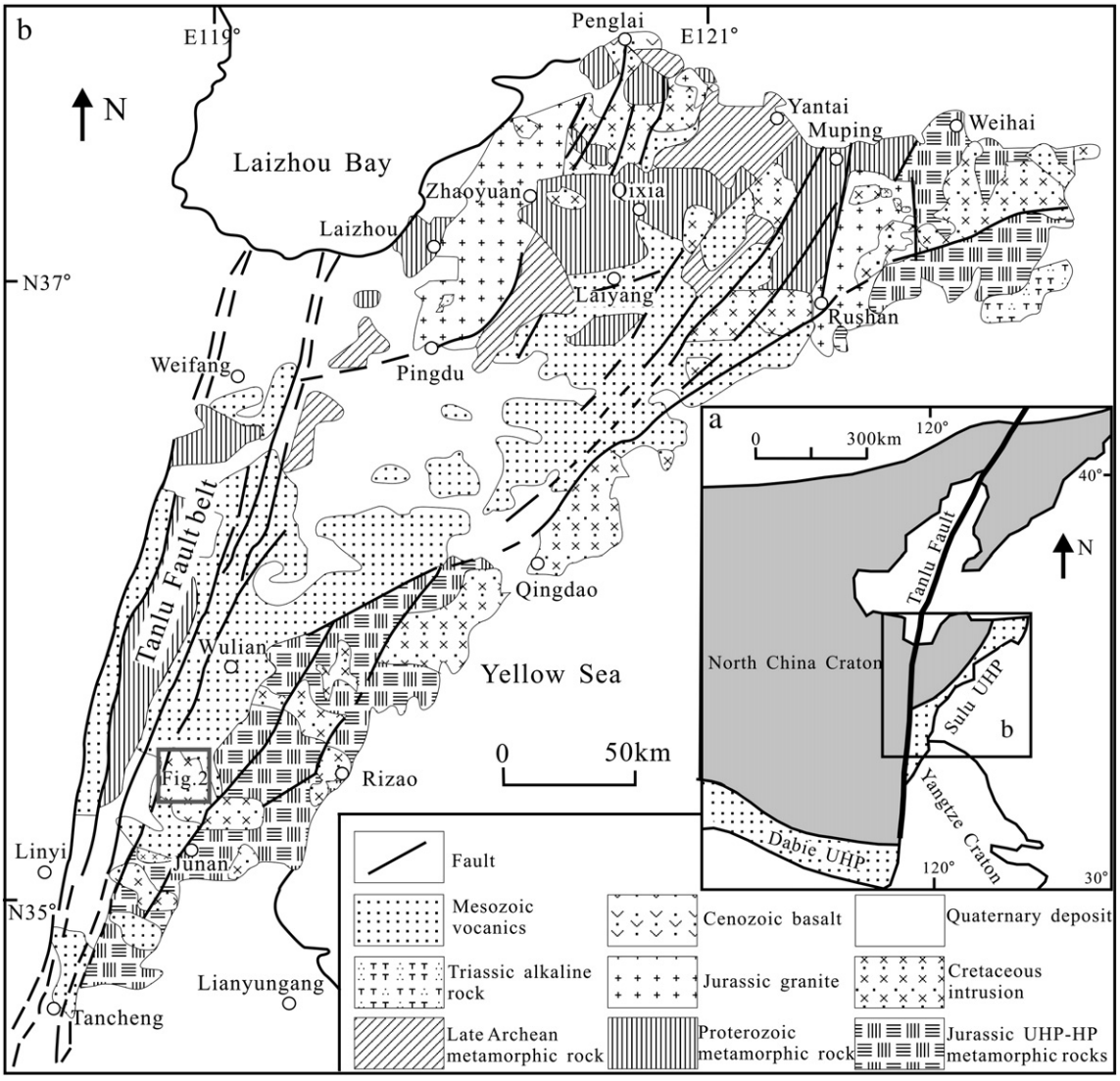

Fig. 1. (a) Simplified geological map showing the major tectonic units in the eastern China. (b) Geological map of the Sulu orogenic belt (after Zhang et al., 2005a).

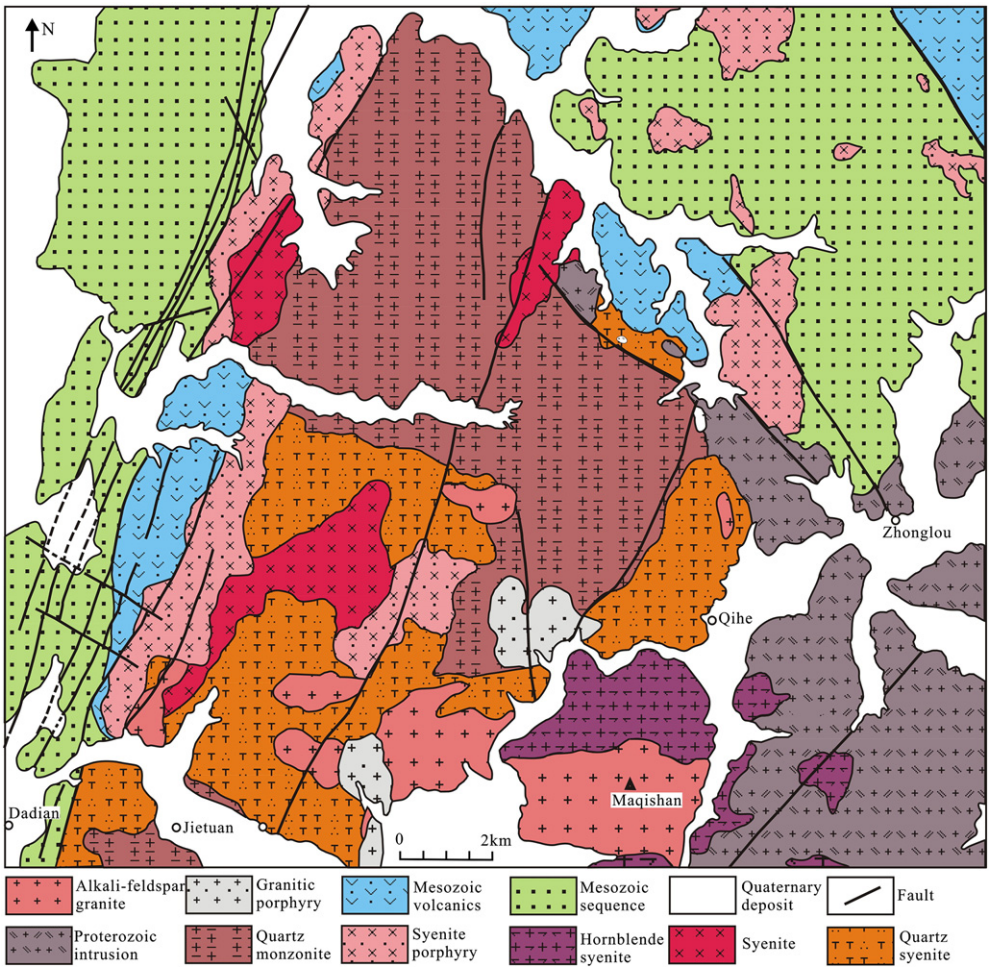

Fig. 2. Geological sketch of the Dadian intrusive complex.

1.5 mm) is platy. Euhedral titanite is the most common accessory mineral in the hornblende syenite. Mafic enclaves are also found within the syenite body.

3.2. Syenite

The syenite is also grayish white and is composed dominantly of feldspar, subordinate quartz, biotite and hornblende and accessory titanite, zircon and magnetite. The subhedral–anhedral feldspars (~95 vol.%, 0.5–4 mm) are perthite, albite and orthoclase. Quartz (<5 vol.%, ~0.5 mm) is irregular. Biotite (<1 vol.%, <0.5 mm) is platy and anhedral. The sporadic hornblende (<0.5 mm) is subhedral–anhedral. Titanite is euhedral and is the most common accessory mineral in the syenite.

3.3. Quartz syenite

The pale red quartz syenite is composed mainly of feldspar and quartz with subordinate biotite and accessory titanite and magnetite. The subhedral–anhedral feldspars (~90 vol.%, 0.1–3 mm) are grainy or irregular and characterized by the intergrowth of orthoclase and albite. Quartz grains (~10 vol.%, 0.05–1 mm) are generally anhedral. Biotite (<1 vol.%, <0.2 mm) is euhedral–subhedral.

3.4. Syenite porphyry

The syenite porphyry is maroon red and is mainly composed of feldspar with subordinate quartz and accessory apatite, magnetite and epidote. The feldspar can be divided into phenocryst and matrix phases according to grain size. The subhedral–anhedral feldspar phenocrysts (~30 vol.%, 0.5–4 mm) are mainly orthoclase. The euhedral–anhedral matrix feldspar (~70 vol.%, 0.1–0.3 mm) is an intergrowth of orthoclase, albite and oligoclase. The sporadic quartz is granular or irregular (<0.2 mm). Some of the feldspars are traversed by secondary calcite veinlets.

4. Analytical methods

Fresh rock samples were prepared in three groups: thin sections for petrography and mineral analyses; 200 micron mesh powder for major, trace element, and Sr–Nd–Pb isotope analyses; and 40–60 micron mesh crushings for zircon separation and U–Pb dating and Hf analyses.

4.1. Mineral compositions and cathodoluminescence (CL) images of zircon grains

Mineral compositions and CL images of zircon grains were obtained using a CAMECA SX50 electron microprobe at the Institute of Geology and Geophysics, Chinese Academy of Sciences (IGGCAS). The operating conditions were 15 kV accelerating voltage and 20 nA beam current.

4.2. Major and trace elements

Major and trace elements were analyzed in the Major and Trace Elements Laboratories of IGGCAS. For major element analyses, mixtures of whole-rock powder (0.5 g) and $Li_2B_4O_7 + LiBO_2$ (5 g)

were heated and fused into glass disks and analyzed by X-ray fluorescence spectroscopy (XRF) with an AXIOS Minerals spectrometer. The analytical uncertainties were generally within 0.1–1% (RSD). Simultaneous analysis of Chinese granite standard GSR1 showed that the accuracy of the results reported is better than 1% (Table 3). Loss on ignition (LOI) was obtained using 0.5 g powder heated up to 1100 °C for 1 h. For trace element analyses, whole-rock powders (40 mg) were dissolved in distilled $HF+HNO_3$ in Teflon screw-cap capsules at 200 °C for 5 days, dried, and then digested with HNO_3 at 150 °C for 1 day, and the final step was repeated. Dissolved samples were diluted to 49 ml with 1% HNO_3 and 1 ml 500 ppb indium was added to the solution as an internal standard. Trace element abundances were determined by inductively coupled plasma mass spectrometry (ICP-MS) using a Finnigan MAT ELEMENT spectrometer. A blank solution was prepared and the total procedural blank was <100 ng for all trace elements. Multi-element standard solution was measured for matrix effects and instrument drift correction. Precision for all trace elements is estimated to be 5% and accuracy is better than 5% for most of the elements as evaluated from the GSR1 standard (Table 3).

4.3. Sr, Nd and Pb isotopes

Whole-rock powders for Sr and Nd isotopic analyses were dissolved in Teflon bombs after being spiked with ^{87}Rb, ^{84}Sr, ^{147}Sm and ^{150}Nd tracers prior to $HF+HNO_3+HClO_4$ dissolution. Rb, Sr, Sm and Nd were separated using conventional ion exchange procedures and measured using a Finnigan MAT262 multi-collector mass spectrometer at the IGGCAS. Detailed descriptions of the analytical techniques are described by Chu et al. (2009). Procedural blanks are <100 pg for Sm and Nd and <300 pg for Rb and Sr. The isotopic ratios were corrected for mass fractionation by normalizing to $^{86}Sr/^{88}Sr=0.1194$ and $^{146}Nd/^{144}Nd=0.7219$, respectively. The measured values for the JNdi-1 Nd standard and NBS987 Sr standard were $^{143}Nd/^{144}Nd=0.512118\pm12$ (2σ, n=10) and $^{87}Sr/^{86}Sr=0.710257\pm12$ (2σ, n=10), respectively. USGS reference material BCR-2 was measured to monitor the accuracy of the analytical procedures, with the following results: $^{143}Nd/^{144}Nd=0.512633\pm13$ (2σ, n=12) and $^{87}Sr/^{86}Sr=0.705035\pm12$ (2σ, n=12).

For Pb isotope determination, the whole-rock powders were dissolved in Teflon vials with purified $HF+HNO_3$ at 120 °C for 7 days and then separated using anion-exchange columns with diluted HBr as elutant. Isotopic ratios were also measured by the Finnigan MAT262 multi-collector mass spectrometer at IGGCAS. Repeated analyses of Pb isotope standard NBS981 yielded $^{206}Pb/^{204}Pb=16.941\pm14$ (n=6), $^{207}Pb/^{204}Pb=15.495\pm14$ (n=6) and $^{208}Pb/^{204}Pb=36.733\pm14$ (n=6).

4.4. Zircon U–Pb dating and in situ Hf isotopic analyses

U–Pb dating and trace element analyses of zircon were conducted synchronously by LA-ICP-MS at the State Key Laboratory of Geological Processes and Mineral Resources, China University of Geosciences, Wuhan. Detailed operating conditions for the laser ablation system and the ICP-MS instrument and data reduction were similar to those described by Liu et al. (2008b, 2010). Laser sampling was performed using a GeoLas 2005 coupled with an Agilent 7500a ICP-MS instrument. A laser spot size of 32 μm and a laser repetition of 6 Hz were used during the analyses. Quantitative calibration for trace element analyses and U–Pb dating were performed by *ICPMSDataCal* (Liu et al., 2008b, 2010). Zircon 91500 was used as external standard for U–Pb dating, and was analyzed twice every 5 analyses. Preferred U–Th–Pb isotopic ratios used for 91500 are from Wiedenbeck et al. (1995). Concordia diagrams and weighted mean calculations were made using Isoplot/Ex_ver 3 (Ludwig, 2003).

In situ zircon Hf isotopic analyses were conducted on the same spots where U–Pb determinations were made. Hf isotopic compositions were determined by a Neptune MC-ICP-MS equipped with GeolasPlus 193 nm ArF excimer laser at the IGGCAS. A laser spot size of 40 μm and a laser repetition of 8 Hz with energy density of 15 J/cm^2 were used during the analyses. The signal collection model was one block with 200 cycles, with an integration time of 0.131 s for 1 cycle and a total time of 26 s during each analyses. Zircon 91500 was used

Table 1
Representative electron microprobe analyses of minerals from the Dadian alkaline complex.

Sample	Feldspar													Hornblende			
	08LX96											08LX100		08LX96			
Spot	1-1	1-2	2	3-2	3-3	5-1	6-1	6-2	7-2	7-3	8-2	2-1	4-3	3-1	4	5	7-1
SiO_2	65.8	67.2	63.8	66.4	65.8	66.6	67.4	65.0	66.1	65.2	65.2	67.5	65.8	50.2	50.5	50.8	50.8
Al_2O_3	18.3	20.7	21.8	20.8	18.4	20.5	20.3	18.1	20.6	18.0	18.1	19.7	20.6	4.55	3.98	4.50	4.24
TiO_2	0.02	0.00	0.00	0.01	0.00	0.01	0.10	0.02	0.00	0.03	0.05	0.00	0.09	0.61	0.58	0.58	0.48
FeO	0.20	0.25	0.18	0.21	0.05	0.20	0.20	0.16	0.26	0.21	0.26	0.11	0.52	13.8	13.0	13.8	13.7
MnO	0.04	0.00	0.00	0.00	0.00	0.00	0.01	0.03	0.02	0.00	0.00	0.06	0.02	1.38	1.41	1.50	1.47
MgO	0.00	0.01	0.01	0.00	0.01	0.04	0.00	0.03	0.02	0.00	0.00	0.02	0.07	14.6	15.1	14.4	14.8
CaO	0.05	1.68	3.60	1.89	0.00	1.71	1.55	0.03	2.02	0.00	0.03	0.24	0.94	10.9	11.0	10.8	11.1
Na_2O	2.08	11.0	9.72	10.6	1.05	10.9	10.8	1.00	10.6	1.58	1.82	11.8	10.7	1.98	1.84	2.06	2.06
K_2O	13.9	0.09	0.15	0.11	15.4	0.22	0.27	15.4	0.21	14.4	14.3	0.12	0.47	0.57	0.53	0.53	0.56
Total	100.4	100.9	99.2	100.0	100.7	100.2	100.6	99.8	99.9	99.6	99.8	99.6	99.3	98.7	98.0	99.0	99.2
	Cations to 8 oxygens													Cations to 23 oxygens			
Si	3.01	2.93	2.84	2.92	3.01	2.93	2.95	3.01	2.92	3.02	3.01	2.97	2.93	7.21	7.28	7.26	7.27
Al	0.99	1.06	1.14	1.08	0.99	1.06	1.05	0.99	1.07	0.98	0.98	1.02	1.08	0.77	0.68	0.76	0.71
Ti	0.00	0.00	0.00	0.00	0.00	0.00	0.00	0.00	0.00	0.00	0.00	0.00	0.00	0.07	0.06	0.06	0.05
Fe^{3+}	0.00	0.00	0.00	0.00	0.00	0.00	0.00	0.00	0.00	0.00	0.00	0.00	0.00	0.66	0.63	0.62	0.58
Fe^{2+}	0.00	0.00	0.00	0.00	0.00	0.00	0.00	0.00	0.00	0.00	0.00	0.00	0.00	1.00	0.94	1.03	1.06
Mn	0.00	0.00	0.00	0.00	0.00	0.00	0.00	0.00	0.00	0.00	0.00	0.00	0.00	0.17	0.17	0.18	0.18
Mg	0.00	0.00	0.00	0.00	0.00	0.00	0.00	0.00	0.00	0.00	0.00	0.00	0.00	3.12	3.24	3.08	3.15
Ca	0.00	0.08	0.17	0.09	0.00	0.08	0.07	0.00	0.10	0.00	0.00	0.01	0.04	1.68	1.70	1.65	1.70
Na	0.18	0.93	0.84	0.90	0.09	0.93	0.91	0.09	0.91	0.14	0.16	1.01	0.92	0.55	0.51	0.57	0.57
K	0.81	0.01	0.01	0.01	0.89	0.01	0.02	0.91	0.01	0.85	0.84	0.01	0.03	0.11	0.10	0.10	0.10
Ab	18.5	91.8	82.3	90.5	9.4	90.9	91.2	9.00	89.4	14.3	16.3	98.2	92.8				
An	0.24	7.72	16.9	8.92	0.00	7.87	7.27	0.15	9.41	0.00	0.16	1.10	4.50				
Or	81.3	0.50	0.82	0.59	90.6	1.20	1.50	90.9	1.18	85.8	83.6	0.67	2.70				
$Mg/(Mg+Fe^{2+})$														0.76	0.78	0.75	0.75

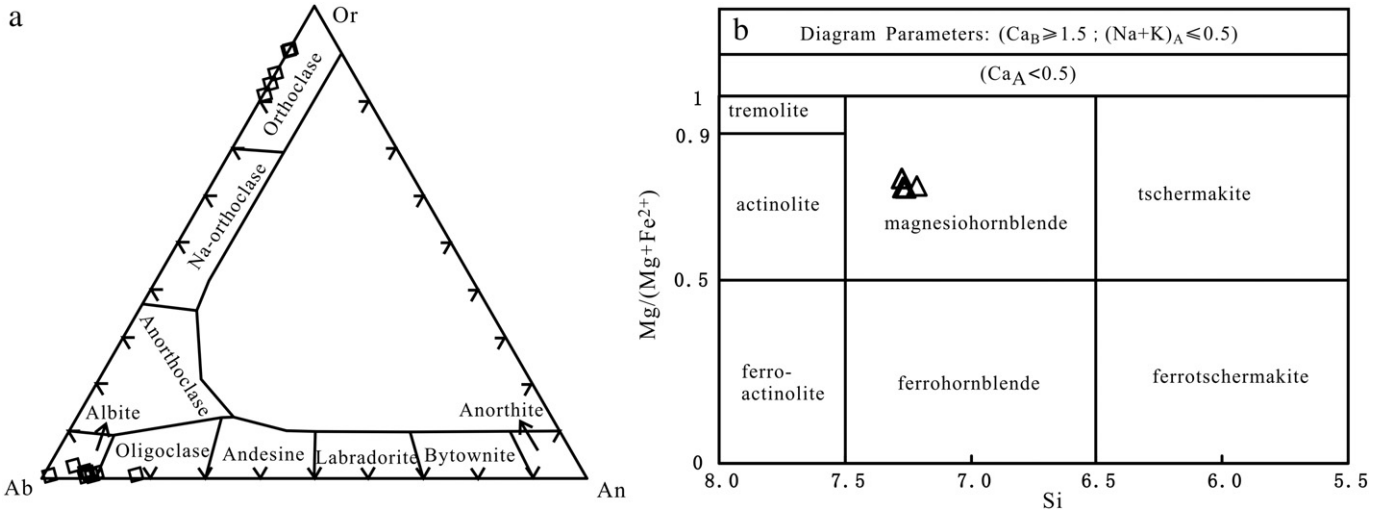

Fig. 3. Classification of feldspar (a) and amphibole (b) from the Dadian alkaline complex. (b) Is after Leake et al. (1997).

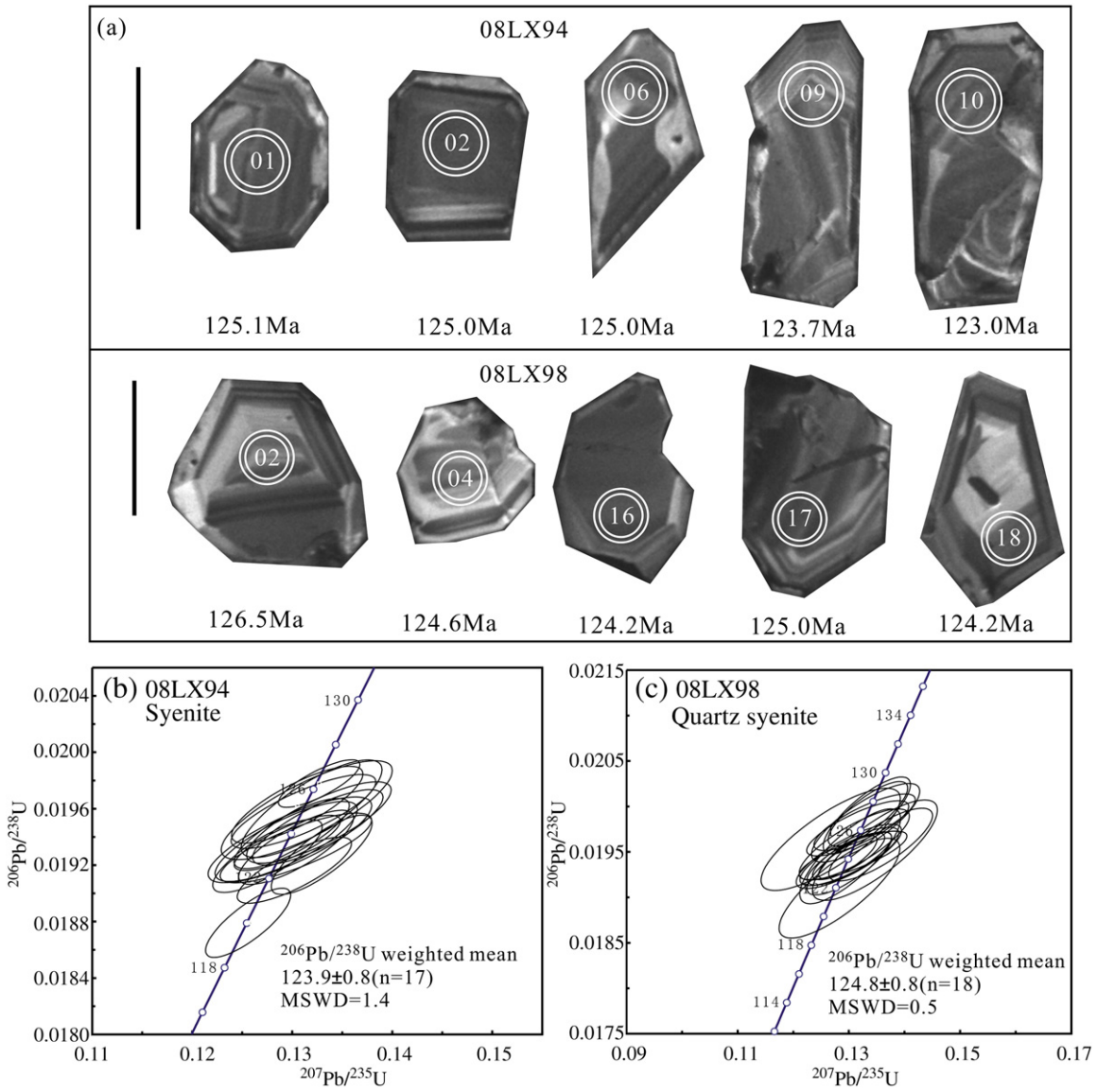

Fig. 4. Representative CL images of zircon grains (a), LA-ICP-MS zircon U–Pb concordia diagrams of syenite (b) and quartz syenite (c) from the Dadian alkaline complex. Large circles represent locations of Hf isotopic analyses, small circles indicate spots of LA-ICP-MS U–Pb dating. The scale bar is 100 μm in (a).

as external standard for Hf isotopic analyses and was analyzed twice every 5 analyses. Replicate analyses of 91500 yielded a mean $^{176}Hf/^{177}Hf$ ratio of 0.282300 ± 24 (2σ, n = 82) which is concordant with the $^{176}Hf/^{177}Hf$ ratios measured by Goolaerts et al. (2004) and Woodhead et al. (2004). The detailed analytical procedures are described in Wu et al. (2006a) and Xie et al. (2008).

5. Results

5.1. Mineral chemistry

Feldspars in the alkaline rocks of the Dadian complex are mostly alkali feldspars enriched in K_2O or Na_2O and can be classified as orthoclase, albite and oligoclase (Table 1 and Fig. 3a). The hornblende is dominantly magnesiohornblende (Fig. 3b) according to the nomenclature of amphiboles recommended by International Mineralogical Association Commission on New Minerals and Mineral Names (Leake et al., 1997). The Al (cations to 23 oxygens) of the hornblende varies from 0.68 to 0.77 p.f.u. (Table 1) which is evidently low.

5.2. Geochronology

Zircon crystals in the syenite (08LX94) are euhedral–subhedral and range from 100 to 200 μm in size, with length to width ratios of 1:1 to 1.5:1. Most grains are transparent to light maroon in color. In the CL images, they are dark and have inconspicuous oscillatory zoning or wide oscillatory zoning in the cores and narrow oscillatory zoning in the rims (Fig. 4a). All the 17 zircons analyzed are concordant and yield a mean $^{206}Pb/^{238}U$ age of 123.9 ± 0.8 Ma (2σ) (Fig. 4b and Table 2). The apparent oscillatory zoning and high Th/U ratios (1.4–4.6) of the zircon grains reveal their magmatic origin. Thus, we interpret the age of 123.9 Ma as the crystallization age of the syenite.

Zircon grains in the quartz syenite (08LX98) are subhedral–anhedral and range from 100 to 250 μm in size, with length to width ratios of 1:1 to 2:1. In the CL images, they typically display gray cores and dark rims, with oscillatory zoning (Fig. 4a). All the 18 zircons analyzed are concordant and yield a mean $^{206}Pb/^{238}U$ age of 124.8 ± 0.8 Ma (2σ) (Fig. 4c and Table 2). Similar to the syenite, the apparent oscillatory zoning and high Th/U ratios (1.2–3.1) of the zircon grains from the quartz syenite reveal their magmatic origin. We therefore consider the age of 124.8 Ma as the crystallization age of the quartz syenite.

The above ages are slightly older than those reported in previous studies on the quartz monzonite and granite (122–123 Ma, Zhou et al., 2003b; Liu et al., 2008a) from the Dadian alkaline complex. Combined with the previous zircon U–Pb ages reported from the Dadian alkaline intrusive complex, we regard that this intrusive complex was emplaced during 122–125 Ma.

5.3. Major oxides and trace elements

Major and trace element analyses are presented in Table 3. All the rocks from Dadian complex show high SiO_2 contents, with a progressive increase in SiO_2 from the syenite porphyry (61.5–62.7 wt.%), hornblende syenite (64.5 wt.%), syenite (66.5–67.5 wt.%) to quartz syenite (69.4–69.7 wt.%). In the R1–R2 diagram, the rocks fall within the fields of syenite and quartz syenite (Fig. 5a). The syenite porphyry shows the highest Al_2O_3 (17.2–17.3 wt.%), whereas

Table 2
LA-ICP-MS U–Pb data of zircons for the Dadian alkaline complex.

Spot	Th (ppm)	U (ppm)	Th/U	Pb (ppm)	$^{207}Pb/^{206}Pb$	1σ	$^{207}Pb/^{235}U$	1σ	$^{206}Pb/^{238}U$	1σ	$^{206}Pb/^{238}U$ (Ma)	1σ
08LX94 (syenite)												
1	410	165	2.48	5.5	0.0493	0.0024	0.1319	0.0058	0.0196	0.0003	125.1	1.8
2	505	181	2.80	6.4	0.0489	0.0023	0.1311	0.0059	0.0196	0.0002	125.0	1.4
3	1658	617	2.69	21.8	0.0486	0.0013	0.1327	0.0033	0.0198	0.0001	126.3	0.9
4	1233	537	2.30	18.5	0.0490	0.0024	0.1304	0.0062	0.0193	0.0002	123.4	1.3
5	1999	435	4.60	19.8	0.0484	0.0016	0.1295	0.0043	0.0194	0.0002	123.6	1.0
6	345	127	2.71	4.5	0.0491	0.0028	0.1315	0.0070	0.0196	0.0003	125.1	1.8
7	1307	412	3.17	16.1	0.0484	0.0021	0.1305	0.0054	0.0196	0.0002	125.3	1.4
8	488	275	1.77	8.0	0.0486	0.0018	0.1299	0.0047	0.0194	0.0002	124.0	1.3
9	402	225	1.79	6.8	0.0491	0.0026	0.1298	0.0067	0.0194	0.0002	123.7	1.6
10	1827	648	2.82	23.4	0.0493	0.0020	0.1326	0.0053	0.0195	0.0002	124.3	1.4
11	415	288	1.44	7.9	0.0481	0.0017	0.1275	0.0045	0.0193	0.0002	123.0	1.3
12	661	176	3.75	7.6	0.0497	0.0023	0.1327	0.0059	0.0195	0.0002	124.5	1.5
13	1651	688	2.40	23.1	0.0500	0.0015	0.1329	0.0041	0.0193	0.0002	123.1	1.5
14	1967	607	3.24	22.8	0.0486	0.0015	0.1256	0.0035	0.0188	0.0002	120.0	1.3
15	466	340	1.37	9.1	0.0491	0.0017	0.1302	0.0047	0.0192	0.0002	122.4	1.2
16	514	346	1.49	9.7	0.0488	0.0023	0.1294	0.0058	0.0194	0.0002	123.7	1.5
17	505	315	1.60	9.0	0.0491	0.0017	0.1304	0.0047	0.0193	0.0002	123.4	1.4
08LX98 (quartz syenite)												
1	150	81	1.87	2.4	0.0502	0.0038	0.1283	0.0089	0.0191	0.0004	122.0	2.8
2	229	119	1.93	3.7	0.0496	0.0030	0.1328	0.0075	0.0198	0.0003	126.6	1.6
3	169	127	1.33	3.5	0.0477	0.0032	0.1310	0.0081	0.0196	0.0003	125.0	2.0
4	132	77	1.72	2.2	0.0513	0.0037	0.1347	0.0092	0.0195	0.0005	124.6	2.9
5	256	158	1.62	4.7	0.0493	0.0024	0.1332	0.0064	0.0199	0.0003	127.0	2.2
6	746	266	2.81	9.7	0.0485	0.0019	0.1299	0.0053	0.0195	0.0002	124.2	1.3
7	278	202	1.38	5.5	0.0485	0.0030	0.1300	0.0077	0.0195	0.0003	124.2	1.8
8	313	171	1.83	5.2	0.0487	0.0024	0.1301	0.0062	0.0194	0.0003	123.7	1.8
9	614	253	2.43	8.5	0.0486	0.0016	0.1298	0.0043	0.0194	0.0002	124.1	1.2
10	304	127	2.39	4.4	0.0493	0.0023	0.1334	0.0058	0.0199	0.0003	127.1	1.8
11	357	116	3.08	4.4	0.0491	0.0025	0.1301	0.0062	0.0194	0.0002	124.0	1.5
12	390	170	2.29	5.8	0.0493	0.0029	0.1330	0.0079	0.0198	0.0004	126.5	2.2
13	367	204	1.80	6.1	0.0484	0.0026	0.1316	0.0075	0.0198	0.0002	126.1	1.6
14	517	318	1.63	9.5	0.0490	0.0030	0.1307	0.0079	0.0195	0.0002	124.3	1.4
15	347	208	1.67	6.0	0.0472	0.0037	0.1267	0.0102	0.0196	0.0005	125.4	2.9
16	294	116	2.54	3.9	0.0495	0.0029	0.1301	0.0073	0.0195	0.0003	124.2	1.7
17	198	102	1.94	3.1	0.0514	0.0031	0.1357	0.0076	0.0196	0.0003	125.0	2.1
18	204	169	1.21	4.2	0.0495	0.0027	0.1302	0.0074	0.0195	0.0004	124.2	2.7

Table 3
Major oxides (wt.%) and trace elements (ppm) for the Dadian alkaline complex.

Rock-type	Syenite		Hornblende syenite		Quartz syenite		Syenite porphyry		Granite	
Sample	08LX94	08LX95	08LX96	10LX33	08LX98	08LX99	08LX100	08LX101	GSR1	GSR1
Latitude	N35°22′17″	N35°22′09″	N35°22′50″	N35°22′52″	N35°22′59″	N35°23′18″	N35°24′00″	N35°24′0″	Avg.	Rem.
Longitude	E118°55′41″	E118°55′51″	E118°55′39″	E118°55′38″	E118°49′43″	E118°49′38″	E118°48′49″	E118°48′48″		
SiO_2	66.5	67.5	64.5	64.1	69.7	69.4	61.5	62.7	73.1	72.8
TiO_2	0.44	0.47	0.51	0.54	0.26	0.33	0.52	0.50	0.28	0.28
Al_2O_3	17.0	16.4	16.9	17.4	15.6	14.5	17.3	17.2	13.4	13.4
FeO^T	1.93	2.02	2.83	3.01	1.69	2.07	3.17	2.97	1.92	1.93
MnO	0.08	0.07	0.10	0.10	0.04	0.04	0.10	0.09	0.06	0.06
MgO	0.25	0.22	0.83	0.94	0.26	0.39	0.94	0.93	0.41	0.42
CaO	0.93	0.67	1.83	2.03	0.69	0.48	2.05	1.78	1.54	1.55
Na_2O	5.80	5.78	5.11	5.14	4.87	5.04	5.06	4.28	3.11	3.13
K_2O	6.00	6.00	5.84	5.92	5.69	5.95	6.21	6.52	5.02	5.01
P_2O_5	0.05	0.04	0.20	0.21	0.06	0.08	0.25	0.23	0.09	0.09
LOI	0.24	0.30	0.44	0.24	0.54	0.94	1.88	1.80	0.69	0.69
Total	99.4	99.7	99.5	100.0	99.6	99.4	99.3	99.4	99.8	99.6
$Mg^{\#}$	18.7	16.2	34.4	35.7	21.5	25.1	34.6	35.8		
Cr	88.6	76.8	68.7	102	112	106	67.8	40.4	2.79	5.00
Co	1.48	1.24	3.94	5.11	1.98	3.44	3.87	3.41	3.40	3.40
Ni	62.1	0.57	1.62	16.9	1.63	2.46	16.05	0.89	3.10	2.30
Cs	1.11	1.35	1.98	1.45	1.77	2.61	3.66	3.49	39.3	38.4
Rb	116	162	165	125	155	229	148	162	481	466
Sr	56.2	37.1	563	523	217	251	483	455	112	106
Ba	174	145	1955	1700	702	794	2834	2640	337	343
La	126	107	180	181	117	129	116	110	53.6	54.0
Ce	286	254	303	303	209	226	209	196	108	108
Pr	34.	31.9	30.9	31.0	22.1	24.9	23.2	21.9	13.3	12.7
Nd	124	121	98.0	100	71.3	81.7	78.6	74.3	48.9	47.0
Sm	23.5	25.6	13.3	13.1	9.89	11.4	12.2	11.6	10.1	9.70
Eu	1.56	1.10	2.47	2.52	1.55	1.34	3.13	3.02	0.85	0.85
Gd	19.4	21.6	11.1	10.8	8.37	9.49	9.49	9.10	9.36	9.30
Tb	2.87	3.17	1.26	1.14	1.01	1.20	1.14	1.11	1.65	1.65
Dy	15.9	18.0	6.06	5.16	5.34	6.39	5.57	5.63	10.7	10.2
Ho	2.94	3.34	1.17	0.99	1.05	1.31	1.07	1.05	2.25	2.05
Er	7.40	8.31	3.25	2.73	2.96	3.76	2.86	2.84	6.97	6.50
Tm	0.97	1.08	0.48	0.40	0.46	0.57	0.42	0.41	1.12	1.06
Yb	5.54	6.43	3.16	2.68	2.94	3.94	2.75	2.67	7.81	7.40
Lu	0.77	0.93	0.48	0.44	0.46	0.62	0.41	0.40	1.25	1.15
Y	71.4	79.9	31.2	26.7	29.0	33.9	27.1	26.4	63.6	62.0
Zr	619	759	662	601	448	385	417	396	170	167
Hf	15.2	18.1	14.9	13.1	12.3	12.3	10.6	10.4	6.50	6.30
Nb	34.5	45.7	29.8	23.9	26.7	47.1	20.0	20.3	41.7	40.0
Ta	2.62	3.37	1.73	1.23	1.88	3.49	1.18	1.22	7.40	7.20
Th	22.6	33.6	31.3	24.9	47.0	74.3	21.4	20.4	55.8	54.0
U	1.78	3.63	3.65	3.56	4.74	8.92	2.63	2.50	18.9	18.8
Pb	27.8	24.4	26.8	23.5	35.7	18.0	26.5	25.3	32.8	31.0
δEu	0.22	0.14	0.6	0.63	0.51	0.38	0.86	0.87		
$(La/Yb)_N$	15.3	11.3	38.5	45.4	26.9	22.1	28.3	27.7		
T_{Zr} (°C)	890	914	891	878	873	847	837	846		

LOI: loss on ignition. $Mg^{\#} = 100 \times Mg/(Mg + \sum Fe)$ atomic ratio. $T_{Zr}(°C) = 12{,}900/[2.95(0.85\,M + \ln(496{,}000/Zr_{melt})$, $M = (Na + K + 2Ca)/(Al \times Si)$ cation ratio (Watson and Harrison, 1983). GSR1 is Chinese granite standard. Avg.: average value measured for reference standard. Rem.: recommended value for reference standard.

the quartz syenite has the lowest Al_2O_3 (14.5–15.6 wt.%). The Al_2O_3 content of hornblende syenite and syenite (16.4–17.0 wt.%) is comparable. Almost all the rocks are metaluminous (Fig. 5b). They also display high and similar Na_2O and K_2O contents ($Na_2O + K_2O = 10.6$–11.8 wt.%), falling in the alkaline field in SiO_2-A.R. diagram (Fig. 5c). However, the K_2O contents are higher than Na_2O ($K_2O/Na_2O = 1.03$–1.52) classifying the rocks into shoshonitic series in the K_2O–SiO_2 diagram (Fig. 5d). The syenite porphyry and hornblende syenite have higher CaO (1.78–2.05 wt.%) and FeO^T (2.83–3.17 wt.%) contents relative to syenite and quartz syenite (CaO = 0.48–0.93 wt.%, $FeO^T = 1.69$–2.02 wt.%). All the rocks have low MgO (0.22–0.93 wt.%), TiO_2 (0.26–0.52 wt.%) and P_2O_5 (0.05–0.25 wt.%) contents. The Mg# (18.7–35.8) is low and shows wide variation.

The concentrations and distribution patterns of REE and trace elements in the Dadian alkaline complex show wide variation (Table 3 and Fig. 6), broadly classifying into three groups. The first group, including hornblende syenite and syenite porphyry, is characterized by high LREE (416–630 ppm), comparatively low HREE (23.2–27.0 ppm), strong fractionation between LREE and HREE ($(La/Yb)_N = 27.7$–38.5), moderate to slight negative Eu anomalies ($\delta Eu = 0.60$–0.87), enrichment of Sr, Ba, Th, U and Pb and depletion of HFSE (Nb, Ta, P and Ti). The second group includes syenite which is also characterized by high LREE (542–594 ppm) but high HREE contents (55.9–62.8 ppm), weak fractionation between LREE and HREE ($(La/Yb)_N = 11.3$–15.3) and strongly negative Eu ($\delta Eu = 0.14$–0.22), Sr and Ba anomalies. The REE and trace element features of the third group which includes quartz syenite overlap between the first and second groups.

5.4. Sr–Nd–Pb isotopes

Sr, Nd and Pb isotopic compositions of hornblende syenite, syenite, quartz syenite and syenite porphyry are presented in Table 4. All these

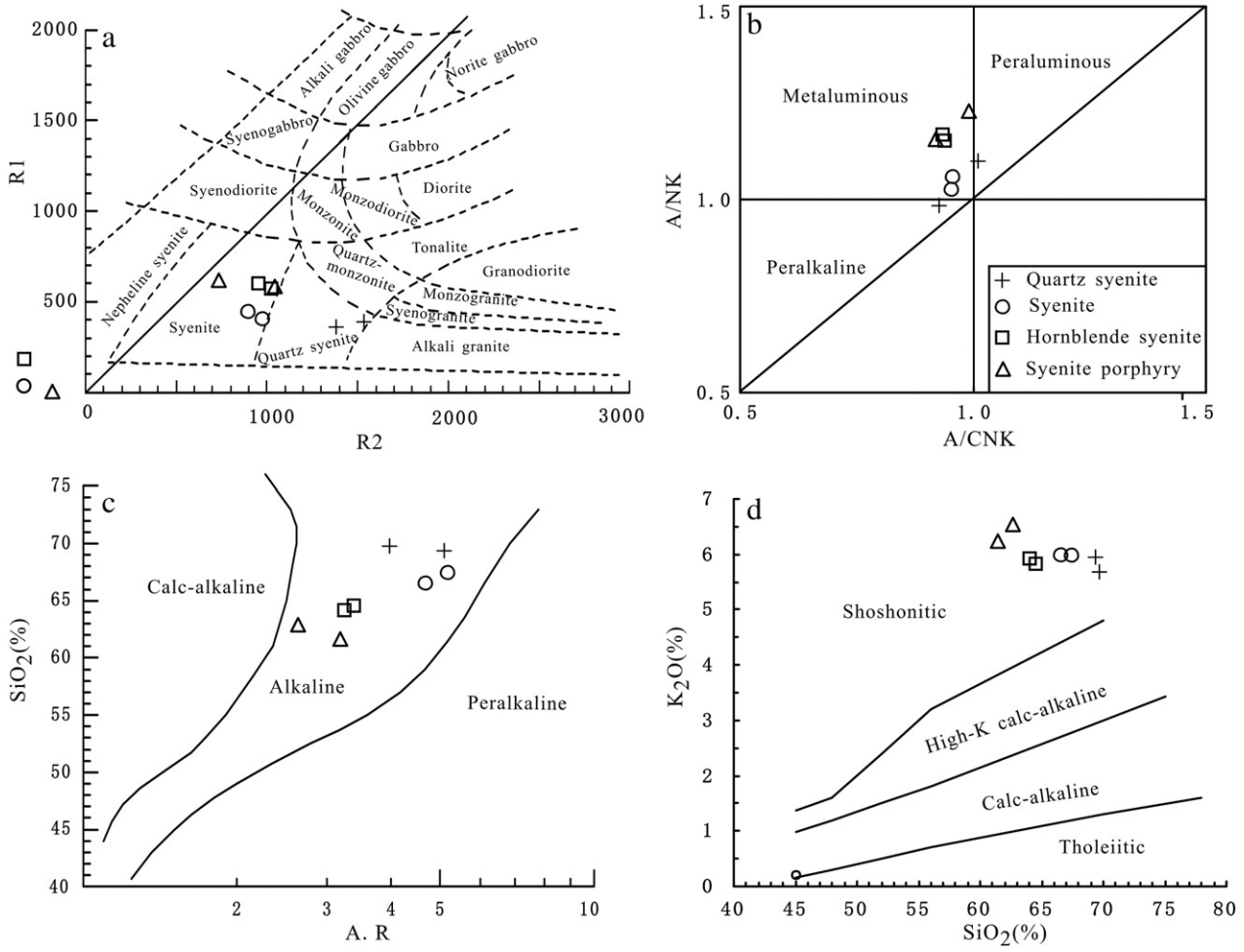

Fig. 5. Plots of (a) R1 vs. R2 [R1 = 4Si−11(Na + K)−2(Fe + Ti), R2 = 6Ca + 2 Mg + Al], (b) A/NK [molar ratio $Al_2O_3/(Na_2O + K_2O)$] vs. A/CNK [molar ratio $Al_2O_3/(CaO + Na_2O + K_2O)$], (c) SiO_2 vs. A.R [$Al_2O_3 + CaO + (Na_2O + K_2O)$]/[$Al_2O_3 + CaO-(Na_2O + K_2O)$] and (d) K_2O vs. SiO_2 for the Dadian alkaline complex. (a) is from De la Roche et al. (1980), (c) is from Wright (1969) and (d) is from Peccerillo and Taylor (1976).

rocks have similar Sr, Nd and Pb isotopic compositions. The $(^{87}Sr/^{86}Sr)_i$ and $\varepsilon_{Nd}(t)$ vary from 0.708505 to 0.708761 and −16.5 to −17.9 respectively. The Pb isotopic compositions are characterized by $(^{206}Pb/^{204}Pb)_i = 16.706–16.779$, $(^{207}Pb/^{204}Pb)_i = 15.427–15.450$ and $(^{208}Pb/^{204}Pb)_i = 37.266–37.352$.

A former study has documented Sr, Nd and Pb isotopic compositions of the quartz monzonite from Dadian alkaline complex as: $(^{87}Sr/^{86}Sr)_i = 0.708132–0.708874$, $\varepsilon_{Nd}(t) = -16.7$ to -17.8, $^{206}Pb/^{204}Pb = 16.938–17.143$, $^{207}Pb/^{204}Pb = 15.315–15.470$ and $^{208}Pb/^{204}Pb = 37.727–38.111$ (Liu et al., 2008a). The present results are broadly concordant with these, except for the wide variation displayed by Sr and Pb isotopic compositions (Table 4).

5.5. Zircon Hf isotope

The results from in situ Hf isotopic analyses of zircons from the Dadian alkaline complex are listed in Table 5 and shown in Fig. 7. There are no major differences in $\varepsilon_{Hf}(t)$ values among the various rock types analyzed in this study. Seventeen analyses obtained from 17 zircons from the syenite (08LX94) yield $^{176}Hf/^{177}Hf$ ratios of 0.282099–0.282239 and $\varepsilon_{Hf}(t)$ values varying from −21.2 to −16.4 with an average value of -19.7 ± 0.7. Eighteen analyses obtained from 18 zircons from the quartz syenite (08LX98) yield $^{176}Hf/^{177}Hf$ ratios of 0.282099–0.282239 and $\varepsilon_{Hf}(t)$ values of −21.2 to −16.4 with an average value of -20.4 ± 0.3.

6. Discussion

6.1. Mantle source and crustal contamination

The Sr–Nd–Pb isotopic compositions of the hornblende syenite, syenite, quartz syenite and syenite porphyry as well as quartz monzonite (Table 4) are different from the lower or upper crust of NCC and YC but are similar to the early Cretaceous mafic dykes from the Sulu orogenic belt (Fig. 8). The Hf isotopic compositions of the Dadian alkaline complex are also concordant with that of the nearby mafic dykes ($\varepsilon_{Hf}(t) = -21.1$ to -23.5, Liu et al., 2008a). We therefore consider that the Dadian alkaline complex shares a similar source as that of the mafic dykes. Furthermore, the existence of mafic enclaves in the hornblende syenite (Fig. 9a) and their interaction with the host rocks (Fig. 9b) suggest that mantle-derived material might have provided the source for the Dadian alkaline complex. It is commonly accepted that these mafic dykes originated from an enriched lithospheric mantle (Yang et al., 2005c; Liu et al., 2008a), suggesting that the Dadian alkaline complex might also be related to an enriched lithospheric mantle source.

However, the markedly high SiO_2 and low MgO, FeO^T and CaO contents indicate that the Dadian alkaline complex experienced strong crystal fractionation or crustal contamination. This is because partial melting of any mantle rocks would generate magmas with low SiO_2 content, though moderate SiO_2 (56–60wt.%) magmas can be produced in case where the mantle is highly enriched in liquid (Zhang

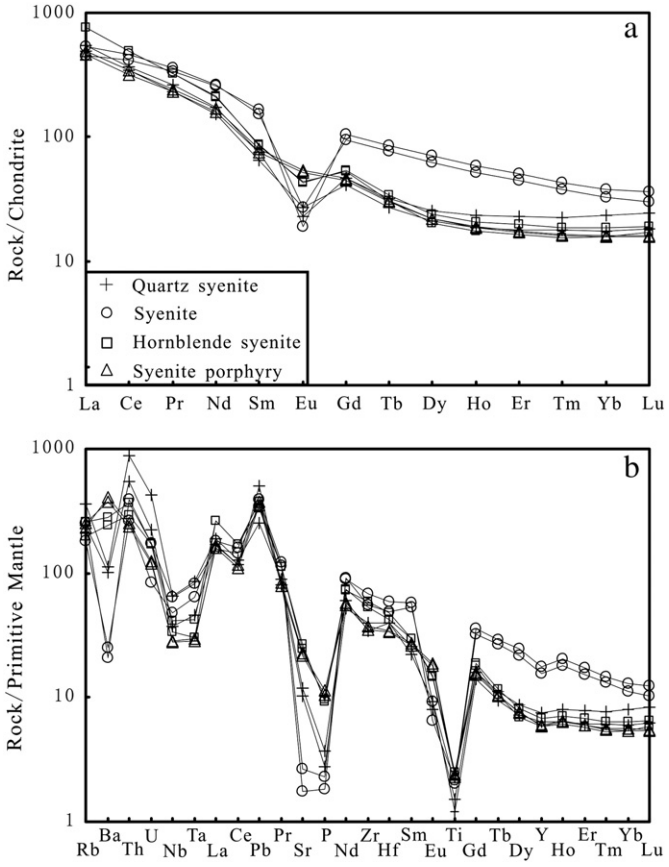

Fig. 6. Chondrite-normalized REE patterns (a) and Primitive Mantle (PM) normalized trace element diagrams (b) for the Dadian alkaline complex. The chondrite and PM values are from Sun and McDonough (1989).

et al., 2008). Crustal contamination is supported by the Sr and Nd isotopic compositions. Except for the syenite porphyry, the distinct positive correlation between SiO_2 and $(^{87}Sr/^{86}Sr)_i$ and negative correlation between SiO_2 and $\varepsilon_{Nd}(t)$ from hornblende syenite to quartz syenite (Fig. 10a and b) suggest that crustal contamination played an important role during magma ascent. The comparatively low $\varepsilon_{Nd}(t)$ and SiO_2 but high $(^{87}Sr/^{86}Sr)_i$ of the syenite porphyry might be related to weak carbonate metasomatism which is also supported by petrographic studies as well as its high CaO content. The lower Nb and Ta concentrations and Nb/Ta ratios of the syenite relative to syenite porphyry and hornblende syenite is better explained by crustal contamination rather than crystal fractionation. Since both Nb and Ta belong to HFSE and have similar geochemical behavior, these elements are not markedly fractionated in most mantle magmatic processes (Liang et al., 2009). Ti-rich minerals such as rutile, titanite and ilmenite are the potential minerals responsible for the distribution and budget of Nb and Ta (Green, 1995; Dostal and Chatterjee, 2000; Ying et al., 2007), and all of them favor Ta over Nb in silicate liquids (Foley et al., 2000; Horng and Hess, 2000; Schmidt et al., 2004; Klemme et al., 2005; Xiong et al., 2005; Bromiley and Reffern, 2008; Liang et al., 2009). This would lead to an increase in the Nb/Ta ratio in the residual melt if fractionation proceeds. However, such a feature is not observed in the Dadian alkaline complex (Fig. 10c). The Nb/Ta ratios of syenite porphyry and hornblende syenite (16.7–19.4) are similar to the mafic dykes in Sulu orogenic belt (average 19.9, Yang et al., 2005c; Tang et al., 2009) whereas the Nb/Ta ratios of syenite and quartz syenite (13.2–14.3) are comparable with crustally derived granites (11.2–13.6, Yang et al., 2005c) and the continental crust (12–13, Barth et al., 2000), indicating that crustal contamination was probably instrumental in the formation of the

Table 4
Sr–Nd–Pb isotopic compositions for the Dadian alkaline complex.

Sample	Age (Ma)	Rb (ppm)	Sr (ppm)	$^{87}Rb/^{86}Sr$	$^{87}Sr/^{86}Sr$ (2σ)	$(^{87}Sr/^{86}Sr)_i$	Sm (ppm)	Nd (ppm)	$^{147}Sm/^{144}Nd$	$^{143}Nd/^{144}Nd$ (2σ)	$\varepsilon_{Nd}(t)$	T_{DM2} (Ma)	$(^{206}Pb/^{204}Pb)i$	$(^{207}Pb/^{204}Pb)i$	$(^{208}Pb/^{204}Pb)i$	Ref.
Syenite																This study
08LX94	124	114.4	57.4	5.7756	0.718790 ± 20	0.708611	18.8	93.5	0.1219	0.511709 ± 12	−17.0	2337	16.718	15.433	37.352	
Hornblende syenite																
08LX96	124	167.4	566.7	0.8551	0.710012 ± 16	0.708505	13.5	99.7	0.0819	0.511700 ± 11	−16.5	2298	16.777	15.440	37.330	
Quartz syenite																
08LX98	124	155.8	212.1	2.1279	0.712392 ± 10	0.708642	8.0	53.6	0.0907	0.511657 ± 10	−17.5	2379	16.779	15.450	37.283	
Syenite porphyry																
08LX101	124	163.2	456.1	1.0362	0.710587 ± 12	0.708761	10.5	70.3	0.0903	0.511634 ± 11	−17.9	2416	16.706	15.427	37.266	Liu et al., 2008a
Quartz monzonite																
DC1-3	124	188.0	813.0	0.5730	0.709142 ± 9	0.708132	11.4	79.0	0.0870	0.511638 ± 9	−17.8	2405	16.938	15.445	37.882	
DC1-5	124	178.0	851.0	0.5200	0.709148 ± 8	0.708232	11.1	74.2	0.0910	0.511647 ± 12	−17.7	2395	16.966	15.470	37.933	
DC1-6	124	169.0	864.0	0.4860	0.709011 ± 11	0.708154	10.7	73.5	0.0880	0.511639 ± 16	−17.8	2404	16.938	15.416	37.727	
DC2-2	124	133.0	1023.0	0.3230	0.709443 ± 10	0.708874	10.1	65.4	0.0930	0.511695 ± 14	−16.8	2321	17.143	15.521	38.111	
DC2-7	124	133.0	1008.0	0.3260	0.709144 ± 12	0.708569	10.7	72.0	0.0900	0.511694 ± 13	−16.7	2319	17.139	15.435	37.846	
DC2-9	124	131.0	1025.0	0.3170	0.709402 ± 8	0.708843	11.1	71.6	0.0930	0.511696 ± 10	−16.7	2319	17.032	15.315	37.744	

Chondrite Uniform Reservoir (CHUR) values ($^{87}Rb/^{86}Sr = 0.0847$, $^{87}Sr/^{86}Sr = 0.7045$, $^{147}Sm/^{144}Nd = 0.1967$, $^{143}Nd/^{144}Nd = 0.512638$) are used for the calculation. $\lambda_{Rb} = 1.42\times10^{-11}$ year^{-1}, $\lambda_{Sm} = 6.54\times10^{-12}$ year^{-1} (Lugmair and Harti, 1978). $\lambda_{U238} = 1.55125\times10-10$ year^{-1}, $\lambda_{U235} = 9.8485\times10^{-10}$ year^{-1}, $\lambda_{Th232} = 4.9475\times10^{-11}$ year^{-1} (Steiger and Jäger, 1977).

Table 5
Zircon Hf isotopic compositions for the Dadian alkaline complex.

Spot	Age (Ma)	$^{176}Yb/^{177}Hf$	$^{176}Lu/^{177}Hf$	$^{176}Hf/^{177}Hf$	2σ	$\varepsilon_{Hf}(0)$	$\varepsilon_{Hf}(t)$	T_{DM1} (Ma)	T_{DM2} (Ma)	$f_{Lu/Hf}$
08LX94 (syenite)										
1	124	0.048785	0.001606	0.282113	0.000022	−23.3	−20.7	1632	2495	−0.95
2	124	0.054338	0.001694	0.282137	0.000025	−22.5	−19.9	1602	2442	−0.95
3	125	0.093874	0.002828	0.282189	0.000026	−20.6	−18.1	1576	2330	−0.91
4	123	0.068408	0.002223	0.282125	0.000033	−22.9	−20.4	1642	2471	−0.93
5	124	0.069437	0.002135	0.282183	0.000023	−20.8	−18.3	1554	2341	−0.94
6	123	0.046853	0.001539	0.282125	0.000022	−22.9	−20.3	1613	2469	−0.95
7	123	0.112151	0.003332	0.282239	0.000026	−18.9	−16.4	1525	2223	−0.90
8	124	0.040568	0.001361	0.282131	0.000018	−22.7	−20.1	1595	2453	−0.96
9	122	0.035932	0.001185	0.282148	0.000019	−22.1	−19.5	1565	2417	−0.96
10	122	0.071626	0.002193	0.282137	0.000022	−22.5	−20.0	1623	2445	−0.93
11	123	0.034404	0.001152	0.282130	0.000022	−22.7	−20.1	1589	2456	−0.97
12	124	0.079274	0.002521	0.282123	0.000026	−22.9	−20.4	1658	2476	−0.92
13	123	0.113606	0.003361	0.282196	0.000023	−20.4	−17.9	1589	2317	−0.90
14	121	0.085766	0.002490	0.282201	0.000023	−20.2	−17.7	1543	2303	−0.92
15	123	0.043668	0.001456	0.282125	0.000019	−22.9	−20.3	1608	2467	−0.96
16	124	0.046122	0.001549	0.282099	0.000019	−23.8	−21.2	1649	2526	−0.95
17	123	0.043616	0.001456	0.282126	0.000020	−22.8	−20.3	1607	2465	−0.96
08LX98 (quartz syenite)										
1	122	0.021058	0.000698	0.282096	0.000023	−23.9	−21.3	1617	2531	−0.98
2	126	0.034622	0.001112	0.282133	0.000020	−22.6	−19.9	1583	2448	−0.97
3	125	0.037997	0.001334	0.282119	0.000023	−23.1	−20.5	1611	2479	−0.96
4	125	0.037874	0.001241	0.282106	0.000022	−23.5	−20.9	1625	2508	−0.96
5	127	0.056103	0.001965	0.282121	0.000030	−23.0	−20.4	1636	2477	−0.94
6	125	0.038540	0.001242	0.282146	0.000021	−22.1	−19.5	1570	2419	−0.96
7	125	0.019452	0.000651	0.282088	0.000017	−24.2	−21.5	1625	2545	−0.98
8	125	0.028752	0.000954	0.282113	0.000024	−23.3	−20.6	1604	2491	−0.97
9	125	0.027939	0.000962	0.282122	0.000023	−23.0	−20.3	1592	2472	−0.97
10	127	0.044181	0.001450	0.282127	0.000021	−22.8	−20.2	1606	2462	−0.96
11	125	0.061978	0.002064	0.282110	0.000024	−23.4	−20.9	1656	2503	−0.94
12	127	0.044423	0.001468	0.282118	0.000023	−23.1	−20.5	1619	2482	−0.96
13	126	0.034715	0.001179	0.282157	0.000021	−21.7	−19.1	1552	2393	−0.96
14	124	0.042318	0.001453	0.282111	0.000022	−23.4	−20.8	1628	2498	−0.96
15	127	0.050282	0.001673	0.282143	0.000024	−22.2	−19.6	1592	2426	−0.95
16	125	0.026344	0.000902	0.282126	0.000019	−22.8	−20.2	1584	2462	−0.97
17	125	0.026549	0.000916	0.282117	0.000020	−23.2	−20.5	1597	2483	−0.97
18	126	0.021879	0.000757	0.282124	0.000020	−22.9	−20.2	1581	2466	−0.98

The following parameters were applied to calculation: $(^{176}Lu/^{177}Hf)_{CHUR}=0.0332$, $(^{176}Hf/^{177}Hf)_{CHUR,\ 0}=0.282772$; $(^{176}Lu/^{177}Hf)_{DM}=0.0384$, $(^{176}Hf/^{177}Hf)_{DM,\ 0}=0.28325$ (Blichert-Toft and Albaréde, 1997; Griffin et al., 2000), ^{176}Lu decay constant $\lambda=1.867\times10^{-11}$ a^{-1} (Söderlund et al., 2004).

syenite and quartz syenite. In addition, the exceptionally high HREE concentrations in the syenite also cannot be explained by fractionation. Fractional crystallization of HREE-rich minerals, such as garnet, zircon and xenotime, will lead to a decrease of HREE in the residual melt. However, such HREE decrease is not supported in the Dadian alkaline complex (Fig. 10d). Alternatively, crustal contamination can reasonably explain the high HREE concentrations in the syenite. In this case, a shallow level crustal source is envisaged with partial melting at low pressure in the absence of garnet to produce high HREE content in the melt.

The positive correlation between CaO and δEu as well as CaO and Sr (Fig. 10e and f) indicates that fractionation of plagioclase might have occurred during magma evolution. However, fractionation of plagioclase alone is inadequate to explain the negative Eu, Sr and Ba anomalies in the syenite because plagioclase fractionation seems to have been negligible between hornblende syenite and syenite as suggested by the very low CaO content and minor CaO variation within these rocks. The strongly negative Eu, Sr and Ba anomalies in the syenite are much more likely to be related to crustal contamination rather than plagioclase fractionation. Experiments show that dehydration melting of calc-alkaline granitoids (e.g., tonalite and a granodiorite) at low pressure ($P\leq4$ kbar) will produce metaluminous A-type granite with negative Eu and Sr anomalies (Patiño Douce, 1997). Crystallization of a low-pressure residual assemblage dominated by plagioclase accounts for the Eu and Sr depletion in the melts. The low CaO, Sr and Eu contents and high FeO^T/MgO (7.74–9.20), TiO_2/MgO (1.76–2.14) and Na/K (0.95–0.98) ratios as well as high HFSE (e.g., Zr, Nb and Y) contents of syenite are similar to A-type granites. Combined with the existence of Neoproterozoic granodiorite and tonalitic gneiss in the study area, it can be deduced that the syenite was contaminated by the melt originated from partial melting of the Precambrian basement rocks at shallow crustal level.

6.2. Estimation of pressure and temperature

Based on Al-in-hornblende barometer (Schmidt, 1992), the crystallization pressure of the Dadian alkaline is estimated to be around 0.23–0.66 kbar. The low pressure values suggest that the alkaline complex crystallized at a shallow crustal level, although this low-Al hornblende is not an appropriate candidate for quantitative pressure estimate because it is easily and strongly affected by temperature (Hollister et al., 1987; Zhao and Wang, 1998). As discussed above, the Dadian alkaline complex was contaminated by crustal material which originated from partial melting of Precambrian basement rocks at low pressure ($P\leq4$ kbar). If this conclusion is valid, the Dadian alkaline complex might have intruded at a depth shallower than 15 km (Yang et al., 2006). Additionally, the low Sr (37.1–56.2 ppm) and high Y (71.4–79.9 ppm) contents of the syenite are similar to the Nanling-type granites which were produced in an extensional environment during the crustal thinning of southeastern China (Zhang et al., 2005c, 2006, 2008).

Zircon saturation thermometry (Watson and Harrison, 1983) provides a simple and robust means of estimating magma temperatures from bulk-rock compositions. The prerequisite for using zircon

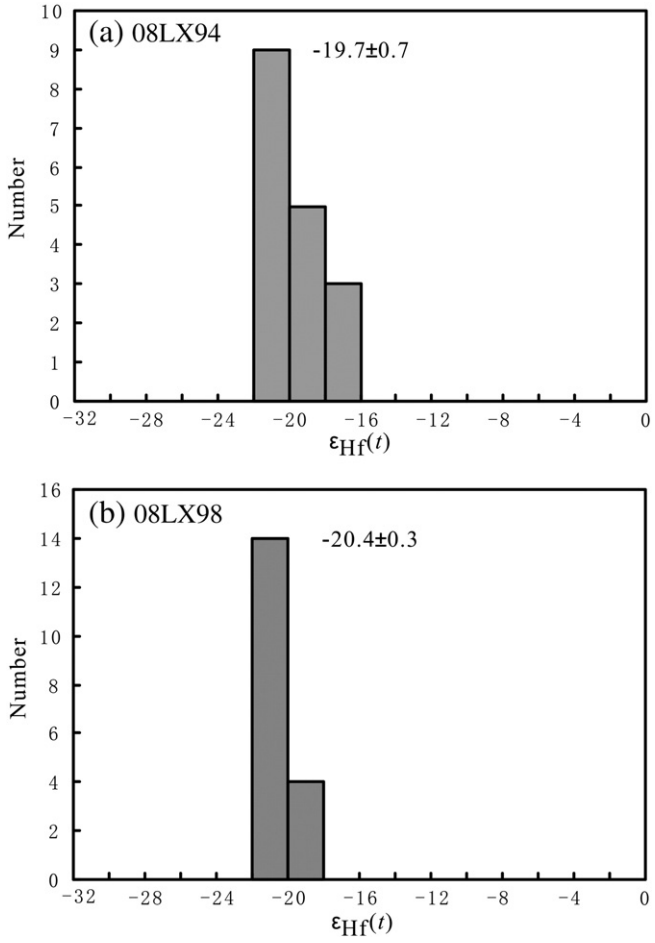

Fig. 7. Zircon Hf isotopic compositions of syenite (a) and quartz syenite (b).

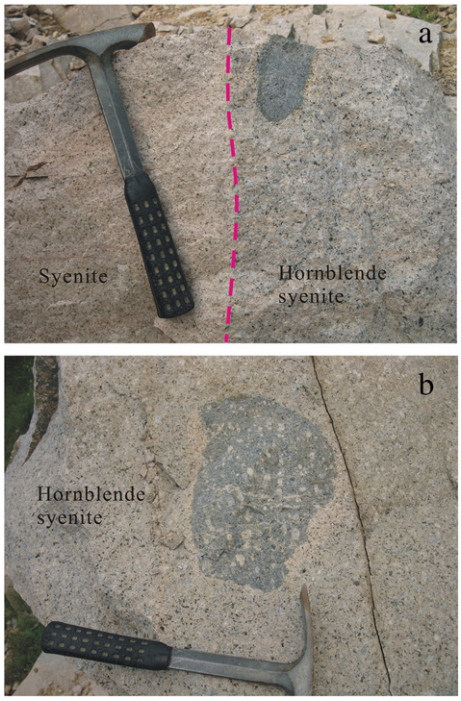

Fig. 9. Mafic enclave captured by hornblende syenite keeps its original composition (a) and is metasomatized by orthoclase (b). Hornblende syenite also cut by syenite in (a).

saturation thermometry is that zirconium is saturated in the melt. The zirconium concentrations of Dadian alkaline complex vary from 385 ppm to 795 ppm with an average value of 527 ppm which is much higher than normal concentrations found in granitic rocks (average 170 ppm, Turekian and Wedepohl, 1961), suggesting that the magma from which the alkaline rocks crystallized was saturated in zirconium. The calculated zircon saturation temperatures (T_{Zr}) of

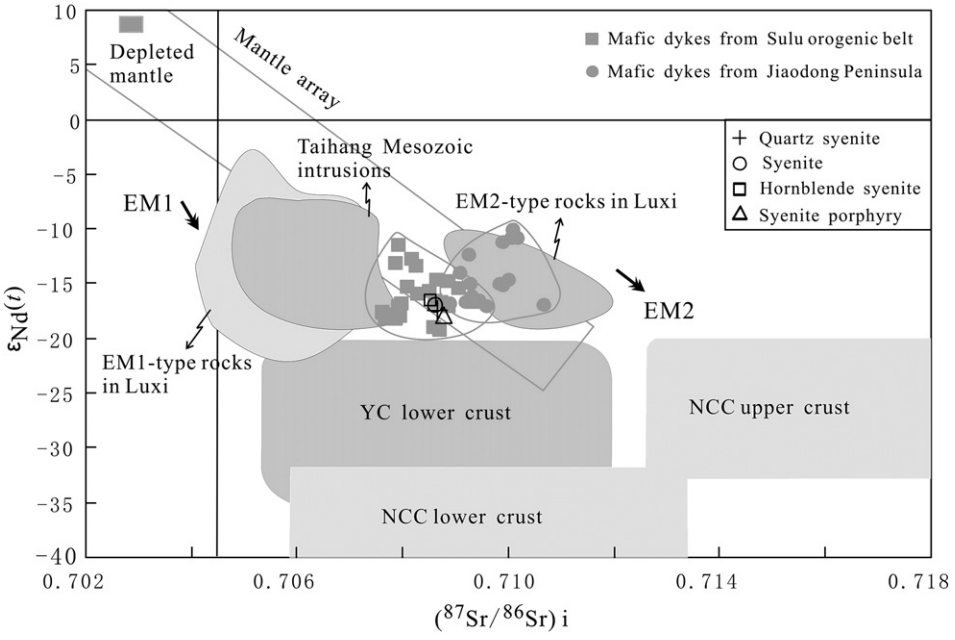

Fig. 8. Initial $^{87}Sr/^{86}Sr$ versus $\varepsilon_{Nd}(t)$ diagram for the Dadian alkaline complex. NCC, North China Craton. YC, Yangtze Craton. The EM1-type rocks in Luxi are from Guo et al. (2001), Yan et al. (2001), Xu et al. (2004a), Yang et al. (2005a), Yang (2007) and Li et al. (2007a). The EM2-type rocks in Luxi are from Zhang et al. (2002), Xu et al. (2004b), Ying et al. (2004) and Yang et al. (2007). The mafic dykes in the Jiaodong Peninsula are from Yang et al. (2004). The mafic dykes in the Sulu orogenic belt are from Yang et al. (2005c) and Liu et al. (2008a). The Mesozoic intrusions of Taihang Mountains are from Chen and Zhai (2003), Chen et al. (2003a, 2004) and Wang et al., 2006). The fields for the lower and upper-middle crust of NCC and lower crust of YC are from Jahn et al. (1999). Mantle array is from Zhang et al. (2005a). DM, EM1 and EM2 are from Zindler and Hart (1986). All the $(^{87}Sr/^{86}Sr)_i$ and $\varepsilon_{Nd}(t)$ values are recalculated to 124 Ma.

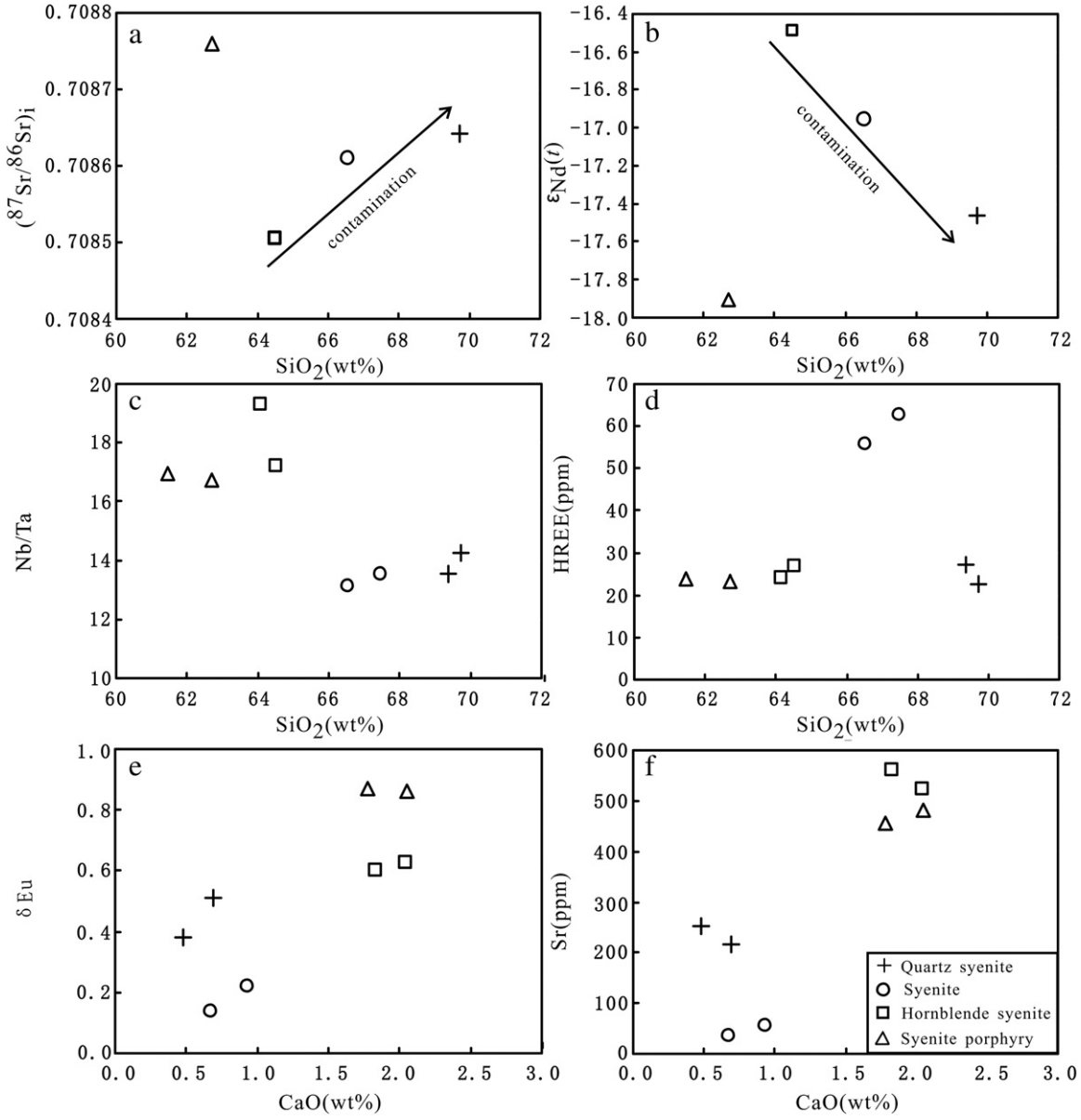

Fig. 10. Plots of ($^{87}Sr/^{86}Sr$) vs. SiO_2 (a), $\varepsilon_{Nd}(t)$ vs. SiO_2 (b), Nb/Ta vs. SiO_2 (c), HREE vs. SiO_2 (d), δEu vs. SiO_2 (e) and Sr vs. CaO (f) for the Dadian alkaline complex.

the syenite, hornblende syenite, quartz syenite and syenite porphyry are 890–914 °C, 878–891 °C, 847–873 °C and 837–846 °C respectively (Table 2), which suggest that the initial temperature of the parent magma might have been higher than 900 °C. This temperature is in accordance with the temperature (950 °C) proposed for the crystallization of A-type granites derived from partial melting of calc-alkaline granitoids at low pressure (Patiño Douce, 1997).

In summary, the Dadian alkaline complex formed at a high temperature but low pressure environment which suggests that the lithosphere of the Sulu orogenic belt may have experienced extensional tectonics in early Cretaceous.

6.3. Petrogenesis

The petrogenesis of syenites involves complex and varied processes in different tectonic settings. The various models proposed can be generally divided into three groups (Yang et al., 2005b and the references therein). Syenite magmas may originate from partial melting of crustal rocks through the influx of volatiles (Miyazaki et al., 2000; Azman, 2001; Martin, 2006) or in a closed system at pressures typical of the base of an over-thickened crust (Harris et al., 1983; Tchameni et al., 2001). The second model considers syenite magmas as products of partial melting of metasomatized/enriched mantle (Litvinovsky et al., 2002; Miyazaki et al., 2003; Conceição and Green, 2004; Wang et al., 2005; Yang et al., 2005b) or differentiation of alkali basalt magma (Brown and Becker, 1986; Xing and Xu, 1994; Macdonald and Scaillet, 2006; Brotzu et al., 2007). The third type of syenites form from magma mixing, particularly the mixing of basic and silicic melts with subsequent differentiation or mixing of mantle-derived silica undersaturated alkali magmas with lower crust derived granitic magmas (Zhao et al., 1995; Brotzu et al., 1997; Stevenson et al., 1997; Vernikovsky et al., 2003; Jung et al., 2007; Ying et al., 2007). Zhao et al. (1995) concluded that the bulk of continental syenites were likely derived by the interaction between mantle-derived alkali basalt magmas and pre-existing continental crust, a process considered as essential for the origin of Si-saturated syenitic compositions. The Sr, Nd and Hf isotopic compositions of Dadian alkaline complex are different from those of the lower and upper crust of NCC and YC, but similar to those of the nearby mafic dykes which were derived from enriched lithospheric mantle. However, the high SiO_2 content

and HREE concentrations and low Nb/Ta ratios of part of the rocks in the Dadian alkaline complex also suggest crustal contamination. High temperature and low pressure indicated by zircon saturation thermometry and Al-in-hornblende barometry from Dadian alkaline complex suggest that the complex formed under high temperature and low pressure conditions. Thus, we conclude that the Dadian alkaline complex was produced from a hot mantle derived magma in shallow crustal level coupled with crustal contamination during magma ascend. It is notable that from hornblende syenite to syenite, the geochemical features evolved from enriched mantle-like to A-type granite affinity, indicating that A-type granites can be produced from enriched lithospheric mantle derived melt via crustal contamination in the Sulu orogenic belt during early Cretaceous. A similar petrogenetic history has also been proposed for the A-type granite in Liaodong Peninsula, as in the case of the early Cretaceous Qianshan A-type granite (Yang et al., 2006).

However, the mechanism of formation of early Cretaceous enriched lithospheric mantle beneath the Sulu orogenic belt remains enigmatic. Some workers regard the lithosphere of Sulu orogenic belt to belong to NCC or YC whereas others consider that it is a unique feature of the Sulu belt (Wang et al., 2004). Pb isotopes are good indicators to distinguish the lithospheric mantle of NCC from YC because the Pb isotopic composition of the lithospheric mantle under the NCC (e.g., Taihang, Luxi, and Jiaodong Peninsula) was less radiogenic than that beneath the YC during the Mesozoic (Xie et al., 2006b) (Fig. 11), though the Pb ratios show an increase from central NCC to southeastern NCC. The Pb isotopic compositions of the Dadian alkaline complex and mafic dykes from Sulu orogenic belt are closer to those for NCC lithospheric mantle than to those of YC (Fig. 11), suggesting that the lithospheric mantle beneath the Sulu orogenic belt likely belongs to the NCC. Models of subduction and delamination were applied to explain the enrichment of the lithospheric mantle. In the subduction model, the enrichment of the lithospheric mantle beneath Sulu orogenic belt was produced by the metasomatism of melts/fluids derived from the subducted Yangtze slab (Guo et al., 2004; Meng et al., 2005; Yang et al., 2005c; Yan et al., 2008; Tang et al.,

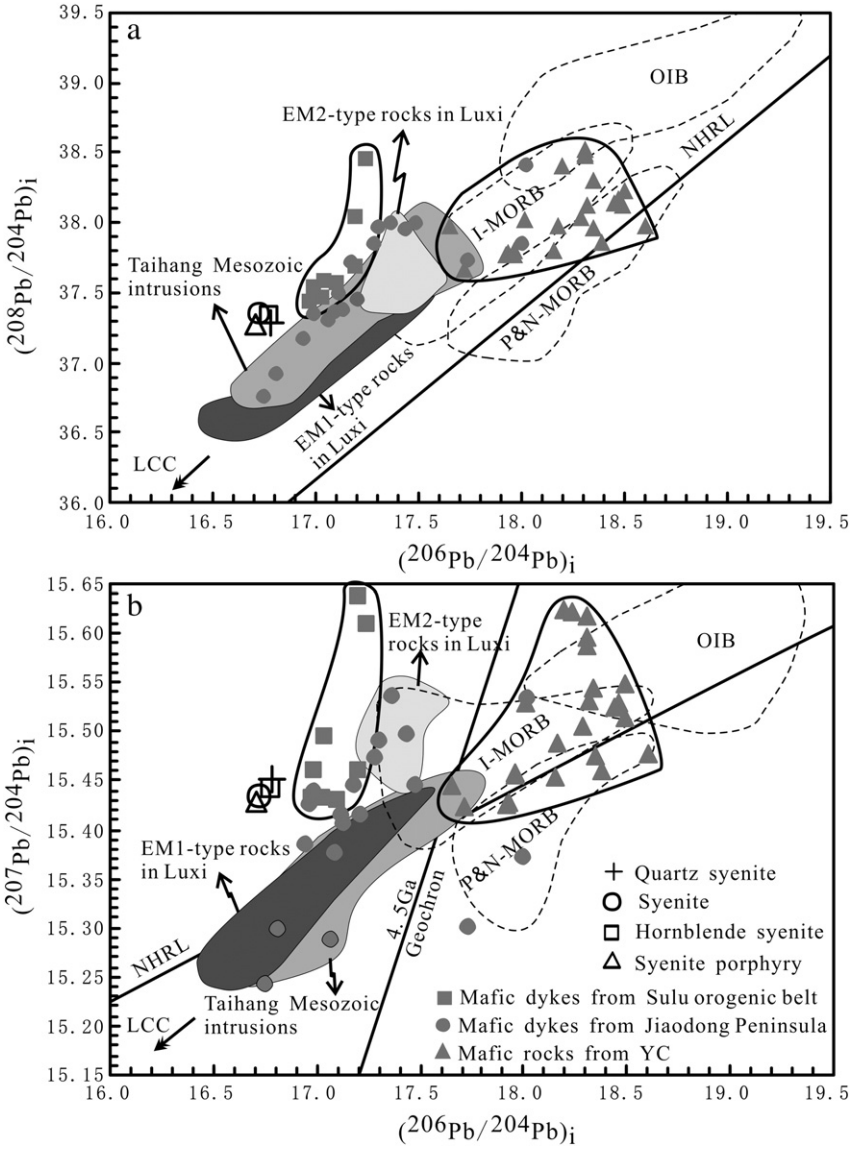

Fig. 11. $^{206}Pb/^{204}Pb$ vs. $^{208}Pb/^{204}Pb$ (a) and $^{206}Pb/^{204}Pb$ vs. $^{207}Pb/^{204}Pb$ (b) diagram for the Dadian alkaline intrusion. The EM1-type rocks in Luxi are represented by Jinan and Zouping gabbros (Guo et al., 2001; Yan et al., 2001; Yang, 2007; Li et al., 2007a). The EM2-type rocks are deputized by Fangcheng basalts (Zhang et al., 2002) and Yinan gabbros (Xu et al., 2004b). The Mesozoic intrusions of Taihang Mountains are from Chen and Zhai (2003), Chen et al. (2003a, 2004) and Wang et al. (2006). The mafic rocks of Yangtze Craton are from Yan et al. (2003, 2005). The mafic dykes in the Sulu orogenic belt and Jiaodong Peninsula are from Liu et al. (2008a) and Yang et al. (2004) respectively. The fields for I-MORB (Indian MORB), P&N-MORB (Pacific and North Atlantic MORB), OIB, NHRL and 4.55 Ga geochron are from Hart (1984), Barry and Kent (1998) and Zou et al. (2000). YC, Yangtze Craton.

2009), whereas in the delamination model the enriched lithospheric mantle was generated by metasomatism of the melts/fluids derived from the foundered lower crust (Liu et al., 2008a; Wang et al., 2009b). The progressive enrichment of the lithospheric mantle from central NCC (e.g., Taihang area) to southeastern NCC (e.g., Luxi area and Jiaodong Peninsula) (Fig. 8), and the old and refractory nature of the lithospheric mantle beneath the Sulu orogenic belt (Yang et al., 2005c; Tang et al., 2009) suggest that the enriched lithospheric mantle might have originated from the ancient lithospheric mantle which was modified by the melts/fluids derived from the subducted Yangtze slab during the Mesozoic (Fig. 12) (Zhang et al., 2005a,b; Lan et al., 2011).

7. Geodynamic implications

Various tectonic models have been proposed to interpret the Mesozoic magmatism in the Sulu orogenic belt. Some researchers regarded that the early Cretaceous magmatism in the Sulu orogenic belt was controlled by the post-collision process which is characterized by the collapse of the orogenic belt or delamination of the lithosphere beneath the orogenic belt (Li et al., 2002, 2005; Guo et al., 2006; Xie et al., 2006a; Xu et al., 2007). Others attribute the magmatism as a product of the large scale lithosphere thinning in eastern China. According to the latter view, the potential geodynamic

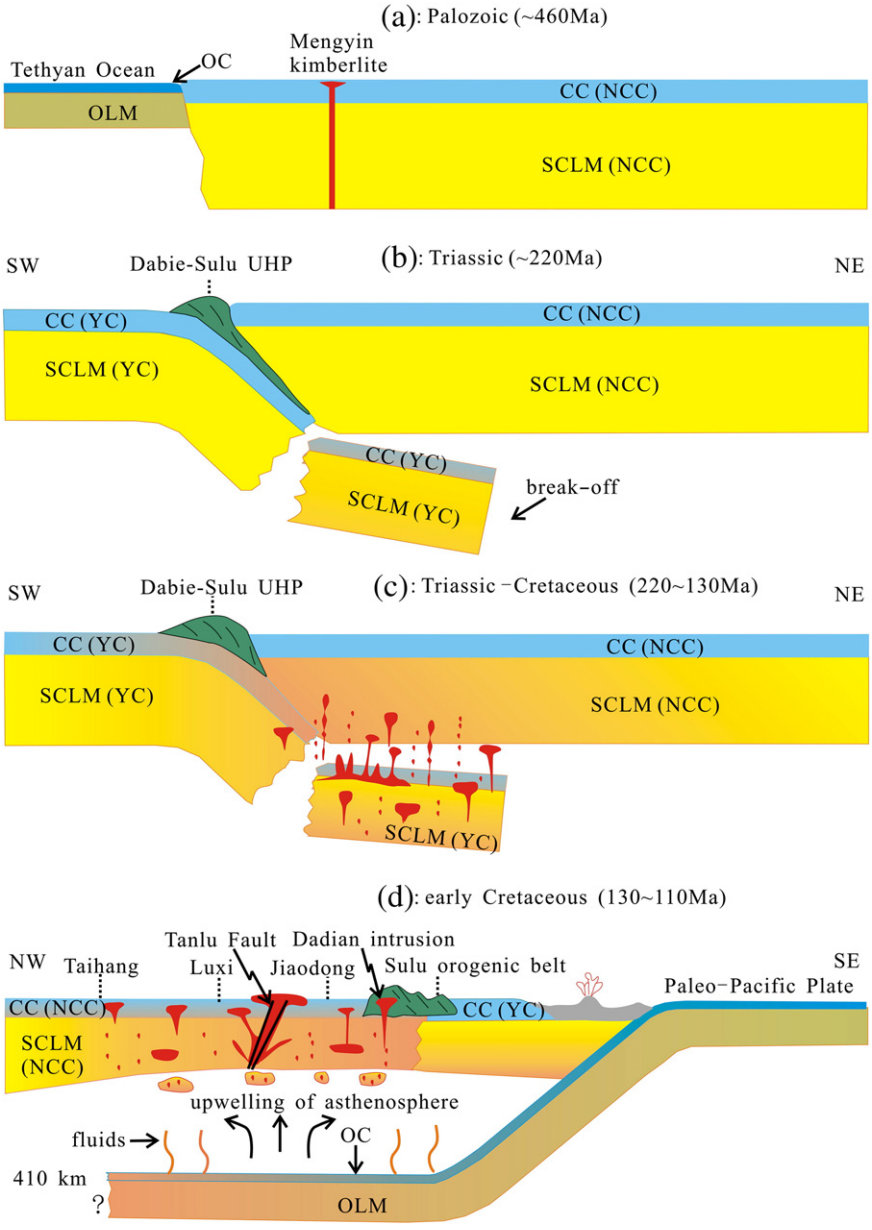

Fig. 12. Schematic sections through the NCC illustrating reactivation of the eastern NCC, transformation of the old cratonic lithosphere to the Mesozoic fertile lithosphere, and lithospheric thinning as a result of subduction-related lithospheric extension and emplacement of related magmas (modified after Zhang et al., 2003 and Chen et al., 2005). (a) Archean well-stratified cratonic lithospheric mantle survived until 460 Ma when the diamondiferous kimberlites erupted; (b) Triassic collision between the Yangtze Craton and the NCC triggered destruction of the NCC lithosphere, simultaneously with the formation of the Dabie–Sulu ultrahigh-pressure metamorphic belt; (c) The subducted Yangtze continental slab produced silicic melts, which modified the overlying refractory lithospheric mantle. Continuous modification by these melts converted the old cratonic lithospheric mantle to Mesozoic enriched lithospheric mantle; (d) Subduction of the paleo-Pacific plate induced lithospheric extension as well as upwelling of asthenosphere, leading to partial melting of the enriched lithospheric mantle and subsequent lithospheric thinning coupled with development of large-scale magmatism. SCLM, subcontinental lithospheric mantle; CC, continental crust; OLM, oceanic lithospheric mantle; OC, oceanic crust; UHP, ultrahigh-pressure rocks; NCC, North China Craton; YC, Yangtze Craton.

forces include the subduction of the paleo-Pacific plate (Hu et al., 2001; Xu et al., 2001; Wu et al., 2005; Ma et al., 2006) or upwelling of a superplume (Zhao et al., 2007; Zhang et al., 2009a). Based on global models for the evolution of orogenic belts, Ma et al. (2006) concluded that it takes about 20–50 Ma from collisional orogeny to collapse of the orogen. Thus the early Cretaceous magmatic activities cannot be explained by the post-collision effect following the continental collision between NCC and YC because of the time lag of more than 100 Ma. In fact, during the early Cretaceous, abundant crustal and mantle derived magmatic rocks formed not only in the Dabie–Sulu orogenic belt, Jiaodong and Liaodong Peninsula, but also in the Taihang and Luxi area, suggesting that these magmatic activities were controlled by a common geodynamic mechanism instead of independent tectonic events. This geodynamic mechanism, therefore, may be related to large scale extension of the lithospheric mantle coupled with upwelling of the asthenosphere. The tectonic framework for the extension of the lithospheric mantle and upwelling of the asthenosphere may be included the post-collisional processes following the Triassic collision between NCC and YC (Li et al., 1993), the Jurassic collision of the Siberian Craton with the NCC-Mongolian continents (Zorin, 1999; Meng, 2003) and the direct effect of paleo-Pacific subduction. Among these, the subduction of the paleo-Pacific slab might have played a crucial role in this process (Sun et al., 2007; Xu et al., 2009). Back-arc extension and sinistral strike-slip movement of the Tan–Lu fault induced by the paleo-Pacific subduction with drifting direction in early Cretaceous may have caused the intense extension of lithospheric mantle and the upwelling of asthenosphere (Zhang et al., 2003; Chen et al., 2005; Zhang et al., 2005b; Sun et al., 2007; Zeng et al., 2009), resulting in the magma generation at shallow crustal levels (Fig. 12). In addition, the superplume model proposed recently is also a viable alternative (Zhao et al., 2007; Zhang et al., 2009a).

8. Conclusions

1. The Dadian alkaline complex crystallized at high temperature and intruded at shallow crustal level during early Cretaceous (122–125 Ma).
2. The alkaline complex was mainly derived from an enriched lithospheric mantle source and contaminated by crustal material during magma ascend. The enriched lithospheric mantle originated from the ancient lithospheric mantle beneath NCC which was modified by the melts/fluids derived from the subducted Yangtze slab. The crustal material was derived from partial melting of Precambrian basement rocks at shallow crustal level.
3. The Dadian alkaline complex bears no relationship to post-orogenic process, but might have been controlled by a common geodynamic mechanism which was instrumental in the development of the early Cretaceous magmatic activities in eastern China. The geodynamic framework was mainly contributed by the paleo-Pacific subduction.

Acknowledgements

This paper was considerably improved by constructive reviews from two anonymous referees. We are grateful to Chao-Feng Li and Xiang-hui Li for help during Sr, Nd and Pb isotope analyses and Zhao-Chu Hu for help during zircon LA ICP-MS U–Pb dating. This study was financially supported by the Natural Science Foundation of China (40625010) and the Crisis Mines Continued Resources Exploration Project of China Geological Survey (20089930).

References

Azman, A.G., 2001. Petrology and geochemistry of granite and syenite from Perhentian Island, Peninsular Malaysia. Geosciences Journal 5, 123–137.
Barry, T.L., Kent, R.W., 1998. Cenozoic magmatism in Mongolia and the origin of central and east Asian basalts. In: Flower, M.F.J., Chung, S.L., Lo, C.H., Lee, T.Y. (Eds.), Mantle Dynamics and Plate Interactions in East Asia. Geodynamics Series. American Geophysical Union, pp. 347–364.
Barth, M.G., McDonough, W.F., Rudnick, R.L., 2000. Tracking the budget of Nb and Ta in the continental crust. Chemical Geology 165, 197–213.
Blichert-Toft, J., Albaréde, F., 1997. The Lu–Hf isotope geochemistry of chondrites and the evolution of the mantle–crust system. Earth and Planetary Science Letters 148, 243–258.
Bonin, B., Azzouni-Sekkal, A., Bussy, F., Ferrag, S., 1998. Alkali-calcic and alkaline post-orogenic (PO) granite magmatism: petrologic constraints and geodynamic settings. Lithos 45, 45–70.
Bromiley, G.D., Reffern, S.A.T., 2008. The role of TiO_2 phases during melting of subduction-modified crust: implications for deep mantle melting. Earth and Planetary Science Letters 267, 301–308.
Brotzu, P., Gomes, C.B., Melluso, L., Morbidelli, L., Morra, V., Ruberti, E., 1997. Petrogenesis of coexisting SiO_2-undersaturated to SiO_2-oversaturated felsic igneous rocks: the alkaline complex of Itatiaia, southeastern Brazil. Lithos 40, 133–156.
Brotzu, P., Melluso, L., Bennio, L., Gomes, C.B., Lustrino, M., Morbidelli, L., Morra, V., Ruberti, E., Tassinari, C., D'Antonio, M., 2007. Petrogenesis of the Early Cenozoic potassic alkaline complex of Morro de São João, southeastern Brazil. Journal of South American Earth Sciences 24, 93–115.
Brown, P.E., Becker, S.M., 1986. Fractionation, hybridisation and magma-mixing in the Kialineq centre East Greenland. Contributions to Mineralogy and Petrology 92, 57–70.
Burke, K., Ashwal, L.D., Webb, S.J., 2003. New way to map old sutures using deformed alkaline rocks and carbonatites. Geology 31, 391–394.
Chen, B., Zhai, M.G., 2003. Geochemistry of late Mesozoic lamprophyre dykes from the Taihang Mountains, north China and implications for the sub-continental lithospheric mantle. Geological Magazine 140, 87–93.
Chen, B., Jahn, B.M., Zhai, M.G., 2003a. Sr–Nd isotopic characteristics of the Mesozoic magmatism in the Taihang–Yanshan orogen, north China craton and implications for Archean lithosphere thinning. Journal of the Geological Society, London 160, 963–970.
Chen, J.F., Xie, Z., Li, H.M., Zhang, X.D., Zhou, T.X., Park, Y.S., Ahn, K.S., Chen, D.G., Zhang, X., 2003b. U–Pb zircon ages for a collision-related K-rich complex at Shidao in the Sulu ultrahigh pressure terrane, China. Geochemical Journal 37, 35–46.
Chen, B., Jahn, B.M., Arakawa, Y., Zhai, M.G., 2004. Petrogenesis of the Mesozoic intrusive complexes from the southern Taihang orogen, North China craton: elemental and Sr–Nd–Pb isotopic constraints. Contributions to Mineralogy and Petrology 148, 489–501.
Chen, B., Tian, W., Zhai, M.G., Arakawa, Y., 2005. Zircon U–Pb geochronology and geochemistry of the Mesozoic magmatism in the Taihang Mountains and other places of the North China craton, with implications for petrogenesis and geodynamic setting. Acta Petrologica Sinica 21, 13–24 (in Chinese with English abstract).
Chu, Z.Y., Wu, F.Y., Walker, R.J., Rudnick, R.L., Pitcher, L., Puchtel, I.S., Yang, Y.H., Wilde, S.A., 2009. Temporal evolution of the lithospheric mantle beneath the eastern North China Craton. Journal of Petrology 50, 1857–1898.
Conceição, R.V., Green, D.H., 2004. Derivation of potassic (shoshonitic) magmas by decompression melting of phlogopite + pargasite lherzolite. Lithos 72, 209–229.
De la Roche, H., Leterrier, J., Granclaude, P., Marchal, M., 1980. A classification of volcanic and plutonic rocks using R1–R2 diagram and major-element analyses—its relationships with current nomenclature. Chemical Geology 29, 183–210.
Dostal, J., Chatterjee, A.K., 2000. Contrasting behaviour of Nb/Ta and Zr/Hf ratios in a peraluminous granitic pluton (Nova Scotia, Canada). Chemical Geology 163, 207–218.
Foley, S.F., Barth, M.G., Jenner, G.A., 2000. Rutile/melt partition coefficients for trace elements and an assessment of the influence of rutile on the trace element characteristics of subduction zone magmas. Geochimica et Cosmochimica Acta 64, 933–938.
Gao, T.S., Chen, J.F., Xie, Z., Yan, J., Qian, H., 2004. Geochemistry of Trassic igneous complex at Shidao in the Sulu UHP metamorphic belt. Acta Petrologica Sinica 20, 1025–1038 (in Chinese with English abstract).
Goolaerts, A., Mattielli, N., Jong, J.D., Weis, D., Scoatea, J.S., 2004. Hf and Lu isotopic reference values for the zircon standard 91500 by MC-ICP-MS. Chemical Geology 206, 1–9.
Green, T.H., 1995. Significance of Nb/Ta as an indicator of geochemical processes in the crust–mantle system. Chemical Geology 120, 347–359.
Griffin, W.L., Pearson, N.J., Belousova, E., Jackson, S.E., Achterbergh, E.V., O'Reilly, S.Y., Shee, S.R., 2000. The Hf isotope composition of cratonic mantle: LA-MC-ICPMS analysis of zircon megacrysts in kimberlites. Geochimica et Cosmochimica Acta 64, 133–147.
Guo, F., Fan, W.M., Wang, Y.J., 2001. Late Mesozoic mafic intrusive complexes in North China Block: constraints on the nature of subcontinental lithospheric mantle. Physics and Chemistry of the Earth (Part A: Solid Earth and Geodesy) 26, 759–771.
Guo, F., Fan, W.M., Wang, Y.J., Zhang, M., 2004. Origin of early Cretaceous calc-alkaline lamprophyres from the Sulu orogen in eastern China: implications for enrichment processes beneath continental collisional belt. Lithos 78, 291–305.
Guo, J.H., Chen, F.K., Zhang, X.M., Siebel, W., Zhai, M.G., 2005. Evolution of syn- to post-collisional magmatism from north Sulu UHP belt, eastern China: zircon U–Pb geochronology. Acta Petrologica Sinica 21, 1281–1301 (in Chinese with English abstract).
Guo, F., Fan, W.M., Li, C.W., 2006. Geochemistry of late Mesozoic adakites from the Sulu belt, eastern China: magma genesis and implications for crustal recycling beneath continental collisional orogens. Geological Magazine 143, 1–13.
Hadj-Kaddour, Z., Liégeois, J.P., Demaiffe, D., Caby, R., 1998. The alkaline–peralkaline granitic post-collisional Tin Zebane dyke swarm (Pan-African Tuareg shield,

Algeria): prevalent mantle signature and late agpaitic differentiation. Lithos 45, 223–243.
Harris, N.B.W., Duyverman, H.J., Almond, D.C., 1983. The trace element and isotope geochemistry of the Sabaloka igneous complex, Sudan. Journal of the Geological Society, London 140, 245–256.
Hart, S.R., 1984. A large-scale isotope anomaly in the southern hemisphere mantle. Nature 309, 753–757.
Hollister, L.S., Grissom, G.C., Peters, E.K., Stowell, H.H., Sisson, V.B., 1987. Confirmation of the empirical correlation of Al in hornblende with pressure of solidification of calc-alkaline plutons. American Mineralogist 72, 231–239.
Horng, W.S., Hess, P.C., 2000. Partition coefficients of Nb and Ta between rutile and anhydrous haplogranite melts. Contributions to Mineralogy and Petrology 138 (2), 176–185.
Hu, S.X., Sun, J.G., Ling, H.F., Ye, Y., Zhai, J.P., Fang, C.Q., 2001. Genetic relationship between eclogite, lamprophyre, gold deposit and enriched mantle of Su–Lu active continental margin in the Mesozoic, China. Acta Petrologica Sinica 17, 425–435 (in Chinese with English abstract).
Huang, J., Zheng, Y.F., Zhao, Z.F., Wu, Y.B., Zhou, J.B., Liu, X.M., 2006. Melting of subducted continent: element and isotopic evidence for a genetic relationship between Neoproterozoic and Mesozoic granitoids in the Sulu orogen. Chemical Geology 229, 227–256.
Jahn, B.M., Wu, F.Y., Lo, C.H., Tsai, C.H., 1999. Crust–mantle interaction induced by deep subduction of the continental crust: geochemical and Sr–Nd isotopic evidence from post-collisional mafic–ultramafic intrusions of the northern Dabie complex, central China. Chemical Geology 157, 119–146.
Jung, S., Hoffer, E., Hoernes, S., 2007. Neo-Proterozoic rift-related syenites (Northern Damara Belt, Namibia): geochemical and Nd–Sr–Pb–O isotope constraints for mantle sources and petrogenesis. Lithos 96, 415–435.
Karmalkar, N.R., Rege, S., Griffin, W.L., O'Reilly, S.Y., 2005. Alkaline magmatism from Kutch, NW India: implications for plume–lithosphere interaction. Lithos 81, 101–119.
Katsube, A., Hayasaka, Y., Santosh, M., Li, S.Z., Terada, K., 2009. SHRIMP zircon U–Pb ages of eclogite and orthogneiss from Sulu ultrahigh-pressure zone in Yangkou area, eastern China. Gondwana Research 15, 168–177.
Kaymakci, N., Aldanmaz, E., Langereis, C., Spell, T.L., Gurer, O.F., Zanetti, K.A., 2007. Late Miocene transcurrent tectonics in NW Turkey: evidence from palaeomagnetism and ^{40}Ar–^{39}Ar dating of alkaline volcanic rocks. Geological Magazine 144, 379–392.
Klemme, S., Prowatke, S., Hametner, K., Gunther, D., 2005. Partitioning of trace elements between rutile and silicate melts: implications for subduction zones. Geochimica et Cosmochimica Acta 69, 2361–2371.
Lan, T.G., Fan, H.R., Hu, F.F., Tomkins, A.G., Yang, K.F., Liu, Y.S., 2011. Multiple crust–mantle interactions for the destruction of the North China Craton: Geochemical and Sr–Nd–Pb–Hf isotopic evidence from the Longbaoshan alkaline complex. Lithos 122, 87–106.
Leake, B.E., Woolley, A.R., Arps, C.E.S., Birch, W.D., Gilbert, M.C., Grice, J.D., Hawthorne, F.C., Kato, A., Kisch, H.J., Krivovichev, V.G., Linthout, K., Laird, J., Mandarino, J.A., Maresch, W.V., Nickel, E.H., Rock, N.M.S., Schumacher, J.C., Smith, D.C., Stephenson, N.C.N., Ungaretti, L., Whittaker, E.J.W., Guo, Y., 1997. Nomenclature of amphiboles: report of the subcommittee on amphiboles of the International Mineralogical Association Commission on New Minerals and Mineral Names. Canadian Mineralogist 35, 219–246.
Li, S.G., Xiao, Y.L., Liou, D.L., Chen, Y.Z., Ge, N.J., Zhang, Z.Q., Sun, S.S., Cong, B.L., Zhang, R.Y., Hart, S.R., Wang, S.S., 1993. Collision of the North China and Yangtze blocks and formation of coesite-bearing eclogites: timing and process. Chemical Geology 109, 89–111.
Li, S.G., Huang, F., Li, H., 2002. Post-collisional lithosphere delamination of the Dabie–Sulu orogen. Chinese Science Bulletin 47, 259–263.
Li, S.G., Li, Q.L., Hou, Z.H., Yang, W., Wang, Y., 2005. Cooling history and exhumation mechanism of the ultrahigh-pressure metamorphic rocks in the Dabie Mountains, central China. Acta Petrologica Sinica 21, 1117–1124 (in Chinese with English abstract).
Li, Q.Z., Xie, Z., Chen, J.F., Gao, T.S., Yu, G., Qian, H., 2007a. Pb–Sr–Nd isotopic characteristics of the gabbros from Jinan and Zouping and the contribution of the lower crust to the magma source. Geological Journal of China Universities 13, 297–310 (in Chinese with English abstract).
Li, X.H., Chen, F.K., Li, C.F., Zhang, H.F., Guo, J.H., Yang, Y.H., 2007b. Zircon ages and Hf isotopic composition gneisses from the Rongcheng ultrahigh-pressure terrain in the Sulu orogeoic belt. Acta Petrologica Sinica 23, 351–368 (in Chinese with English abstract).
Li, S.Z., Kusky, T.M., Liu, X., Zhang, G., Zhao, G., Li, W., Wang, Y., 2009. Two-stage collision related extrusion of the western Dabie HP–UHP metamorphic terranes, central China: evidence from quartz c-axis fabrics and structures. Gondwana Research 16, 294–309.
Liang, J.L., Ding, X., Sun, X.M., Zhang, Z.M., Zhang, H., Sun, W.D., 2009. Nb/Ta fractionation observed in eclogites from the Chinese Continental Scientific Drilling Project. Chemical Geology 268, 27–40.
Liégeois, J.P., Navez, J., Hertogen, J., Black, R., 1998. Contrasting origin of post-collisional high-K calc-alkaline and shoshonitic versus alkaline and peralkaline granitoids. The use of sliding normalization. Lithos 45, 1–28.
Litvinovsky, B.A., Jahn, B.M., Zanvilevich, A.N., Shadaev, M.G., 2002. Crystal fractionation in the petrogenesis of an alkali monzodiorite–syenite series: the Oshurkovo plutonic sheeted complex, Transbaikalia, Russia. Lithos 64, 97–130.
Liu, S., Hu, R.Z., Gao, S., Feng, C.X., Qi, Y.Q., Wang, T., Feng, G.Y., Coulson, L.M., 2008a. U–Pb zircon age, geochemical and Sr–Nd–Pb–Hf isotopic constraints on age and origin of alkaline intrusions and associated mafic dikes from Sulu orogenic belt, Eastern China. Lithos 106, 365–379.
Liu, Y.S., Hu, Z.C., Gao, S., Günther, D., Xu, J., Gao, C.G., Chen, H.H., 2008b. In situ analysis of major and trace elements of anhydrous minerals by LA-ICP-MS without applying an internal standard. Chemical Geology 257, 34–43.
Liu, Y.S., Gao, S., Hu, Z.C., Gao, C.G., Zong, K., Wang, D., 2010. Continental and oceanic crust recycling-induced melt–peridotite interactions in the Trans-North China Orogen: U–Pb dating, Hf isotopes and trace elements in zircons of mantle xenoliths. Journal of Petrology 51, 537–571.
Ludwig, K.R., 2003. User's Manual for Isoplot 3.00, a Geochronological Toolkit for Microsoft Excel, 4. Berkeley Geochronlogical Center Special Publication, pp. 25–32.
Lugmair, G.W., Harti, K., 1978. Lunar initial $^{143}Nd/^{144}Nd$: differential evolution of the lunar crust and mantle. Earth and Planetary Science Letters 39, 349–357.
Ma, C.Q., She, Z.B., Zhang, J.Y., Zhang, C., 2006. Crustal roots, orogenic heat and magmatism. Earth Science Frontiers 13, 130–139 (in Chinese with English abstract).
Macdonald, R., Scaillet, B., 2006. The central Kenya peralkaline province: insights into the evolution of peralkaline salic magmas. Lithos 91, 59–73.
Martin, R.F., 2006. A-type granites of crustal origin ultimately result from open-system fenitization-type reactions in an extensional environment. Lithos 91, 125–136.
Mchone, J.G., 1996. Constraints on the mantle plume model for Mesozoic alkaline intrusions in northeastern North America. The Canadian Mineralogist 34, 325–334.
Melluso, L., Sethna, S.F., D'Antonio, M., Javeri, P., Bennio, L., 2002. Geochemistry and petrogenesis of sodic and potassic mafic alkaline rocks in the Deccan Volcanic province, Mumbai Area (India). Mineralogy and Petrology 74, 323–342.
Meng, Q.R., 2003. What drove late Mesozoic extension of the northern China–Mongolia tract? Tectonophysics 369, 155–174.
Meng, F.C., Xue, H.M., Li, T.F., Yang, H.R., Liu, F.L., 2005. Enriched characteristics of Late Mesozoic mantle under the Sulu orogenic belt: geochemical evidence from gabbro in Rushan. Acta Petrologica Sinica 21, 1583–1592 (in Chinese with English abstract).
Miyazaki, T., Kagami, H., Shuto, K., Mohan, V.R., Rajasekaran, K.C., 2000. Rb–Sr geochronology, Nd–Sr isotopes and whole rock geochemistry of Yelagiri and Sevattur syenites, Tamil Nadu, South India. Gondwana Research 3, 39–53.
Miyazaki, T., Kagami, H., Mohan, V.R., Shuto, K., Morikiyo, T., 2003. Enriched subcontinental lithospheric mantle in the northern part of the South Indian Granulite Terrain: evidence from Yelagiri and Sevattur syenite plutons, Tamil Nadu, South India. Gondwana Research 6, 585–594.
Muñoz, M., Sagredo, J., de Ignacio, C., Fernandez-Suarez, J., Jeffries, T.E., 2005. New data (U–Pb, K–Ar) on the geochronology of the alkaline–carbonatitic association of Fuerteventura, Canary Islands, Spain. Lithos 85, 140–153.
Nédélec, A., Stephens, W.E., Fallick, A.E., 1995. The Panafrican stratoid granites of Madagascar: alkaline magmatism in a post-collisional extensional settings. Journal of Petrology 36, 1367–1391.
Oyhantçabal, P., Siegesmund, S., Wemmer, K., Frei, R., Layer, P., 2007. Post-collisional transition from calc-alkaline to alkaline magmatism during transcurrent deformation in the southernmost Dom Feliciano Belt (Braziliano-Pan-African, Uruguay). Lithos 98, 141–159.
Patiño Douce, A.E., 1997. Generation of metaluminous A-type granites by low-pressure melting of calc-alkaline granitoids. Geology 25, 743–746.
Peccerillo, A., Taylor, S.R., 1976. Geochemistry of Eocene calc-alkaline volcanic rocks from the Kastamonu, northern Turkey. Contributions to Mineralogy and Petrology 58, 63–81.
Peccerillo, A., Barberio, M.R., Yirgu, G., Ayalew, D., Barbieri, M., Wu, T.W., 2003. Relationships between mafic and peralkaline silicic magmatism in continental rift settings: a petrological, geochemical and isotopic study of the Gedesma Volcano, Central Ethiopian Rift. Journal of Petrology 44, 2003–2032.
Ridolfi, F., Renzulli, A., Macdonald, R., Upton, B.G.J., 2006. Peralkaline syenite autoliths from Kilombe volcano, Kenya Rift Valley: evidence for subvolcanic interaction with carbonatitic fluids. Lithos 91, 373–392.
Schmidt, M.W., 1992. Amphibole composition in tonalite as a function of pressure: an experimental calibration of the Al-in-hornblende barometer. Contributions to Mineralogy and Petrology 110, 304–310.
Schmidt, M.W., Dardon, A., Chazot, G., Vannucci, R., 2004. The dependence of Nb and Ta rutile–melt partitioning on melt composition and Nb/Ta fractionation during subduction processes. Earth and Planetary Science Letters 226, 415–432.
Shellnutt, J.G., Zhou, M.F., 2008. Permian, rifting related fayalite syenite in the Panxi region, SW China. Lithos 101, 54–73.
Siebel, W., Danišík, M., Chen, F., 2009. From emplacement to unroofing: thermal history of the Jiazishan gabbro, Sulu UHP terrane, China. Mineralogy and Petrology 96, 163–175.
Söderlund, U., Patchett, P.J., Vervoort, J.D., Isachsen, C.E., 2004. The ^{176}Lu decay constant determined by Lu–Hf and U–Pb isotope systematics of Precambrian mafic intrusions. Earth and Planetary Science Letters 219, 311–324.
Srivastava, R.K., Heaman, L.M., Sinha, A.K., Shihua, S., 2005. Emplacement age and isotope geochemistry of Sung Valley alkaline–carbonatite complex, Shillong Plateau, northeastern India: implications for primary carbonate melt and genesis of the associated silicate rocks. Lithos 81, 33–54.
Steiger, R.H., Jäger, E., 1977. Subcommission on geochronology: convention on the use of decay constants in geo- and cosmochronology. Earth and Planetary Science Letters 36, 359–362.
Stevenson, R., Upton, B.G.J., Steenfelt, A., 1997. Crust–mantle interaction in the evolution of the Ilímaussaq Complex, South Greenland: Nd isotopic studies. Lithos 40, 189–202.
Sun, S.S., McDonough, W.F., 1989. Chemical and isotopic systematics of oceanic basalts: implications for mantle composition and processes. In: Saunders, A.D., Norry, M.J. (Eds.), Magmatism in the Oceanic Basalts. Geological Society Special Publication, pp. 313–345.

Sun, W.D., Ding, X., Hu, Y.H., Li, X.H., 2007. The golden transformation of the Cretaceous plate subduction in the west Pacific. Earth and Planetary Science Letters 262, 533–542.
Tang, H.Y., Zheng, J.P., Yu, C.M., 2009. Age and composition of the Rushan intrusive complex in the northern Sulu orogen, eastern China: petrogenesis and lithospheric mantle evolution. Geological Magazine 146, 199–215.
Tchameni, R., Mezger, K., Nsifa, N.E., Pouclet, A., 2001. Crustal origin of early Proterozoic syenites in the Congo Craton (Ntem Complex), South Cameroon. Lithos 57, 3–42.
Turekian, K.K., Wedepohl, K.H., 1961. Distribution of the elements in some major units of the Earth's crust. Geological Society of America Bulletin 72, 175–192.
Upadhyay, D., Raith, M.M., Mezger, K., Hammerschmidt, K., 2006. Mesoproterozoic rift-related alkaline magmatism at Elchuru, Prakasam Alkaline Province, SE India. Lithos 89, 447–477.
Vernikovsky, V.A., Pease, V.L., Vernikovskaya, A.E., Romanov, A.P., Gee, D.G., Travin, A.V., 2003. First report of early Triassic A-type granite and syenite intrusions from Taimyr: product of the northern Eurasian superplume? Lithos 66, 23–36.
Wang, D.Z., Zhao, G.T., Qiu, J.S., 1995. The tectonic constraint on the late Mesozoic A-type granitoids in eastern China. Geological Journal of Universities 1, 13–21 (in Chinese with English abstract).
Wang, P.C., Zhang, G.R., Xu, H.Y., Liu, J.W., Song, Z.Y., 2004. On geotectonic property of the Su–Lu orogen basement-taking Rongcheng–Weihai sector as an example. Geological Survey and Research 27, 239–244 (in Chinese with English abstract).
Wang, Q., Li, J.W., Jian, P., Zhao, Z.H., Xiong, X.L., Bao, Z.W., Xu, J.F., Li, C.F., Ma, J.L., 2005. Alkaline syenites in eastern Cathaysia (South China): link to Permian–Triassic transtension. Earth and Planetary Science Letters 230, 339–354.
Wang, Y.J., Fan, W.M., Zhang, H.F., Peng, T.P., 2006. Early Cretaceous gabbroic rocks from the Taihang Mountains: implications for a paleosubduction-related lithospheric mantle beneath the central North China Craton. Lithos 86, 281–302.
Wang, S.J., Wang, L.M., Wan, Y.S., Zhang, C.J., Song, Z.Y., Wang, J.G., 2009a. Study on intrusive rocks forming period and stages division in Ludong area. Shandong Land and Resources 25, 8–20 (in Chinese with English abstract).
Wang, T., Liu, S., Hu, R.Z., Feng, C.X., Qi, Y.Q., Feng, G.Y., Wang, C.H., 2009b. Elemental geochemistry and petrogenesis of A-type granites in the Sulu orogen. Journal of Jilin University (Earth Science Edition) 39, 676–688 (in Chinese with English abstract).
Watson, E.B., Harrison, T.M., 1983. Zircon saturation revisited: temperature and composition effects in a variety of crustal magma types. Earth and Planetary Science Letters 64, 295–304.
Wei, C.S., Zheng, Y.F., Zhao, Z.F., 2001. Nd–Sr–O isotopic geochemistry constraints on the age and origin of the A-type granites in eastern China. Acta Petrologica Sinica 17, 95–111 (in Chinese with English abstract).
Wiedenbeck, M., Alle, P., Corfu, F., Griffin, W.L., Meier, M., Oberli, F., Quadt, A.V., Roddick, J.C., Spiegel, W., 1995. Three natural zircon standards for U–Th–Pb, Lu–Hf, trace element and REE analyses. Geostandards and Geoanalytical Research 19, 1–23.
Woodhead, J., Hergt, J., Shelley, M., Eggins, S., Kemp, R., 2004. Zircon Hf-isotope analysis with an excimer laser, depth profiling, ablation of complex geometries and concomitant age estimation. Chemical Geology 209, 121–135.
Wright, J.B., 1969. A simple alkalinity ratio and its application to questions of non-orogenic granite genesis. Geological Magazine 106, 370–384.
Wu, F.Y., Lin, J.Q., Wilde, S.A., Zhang, X.O., Yang, J.H., 2005. Nature and significance of the Early Cretaceous giant igneous event in eastern China. Earth and Planetary Science Letters 233, 103–119.
Wu, F.Y., Yang, Y.H., Xie, L.W., Yang, J.H., Xu, P., 2006. Hf isotopic compositions of the standard zircons and baddeleyites used in U–Pb geochronology. Chemical Geology 234, 105–126.
Xie, Z., Zheng, Y.F., Zhao, Z.F., Wu, Y.B., Wang, Z.R., Chen, J.F., Liu, X.M., Wu, F.Y., 2006a. Mineral isotope evidence for the contemporaneous process of Mesozoic granite emplacement and gneiss metamorphism in the Dabie orogen. Chemical Geology 231, 214–235.
Xie, Z., Li, Q.Z., Gao, T.S., 2006b. Comment on "Petrogenesis of post-orogenic syenites in the Sulu orogenic belt, east China: geochronological, geochemical and Nd–Sr isotopic evidence" by Yang et al. Chemical Geology 235, 191–194.
Xie, L.W., Zhang, Y.B., Sun, J.F., Wu, F.Y., 2008. In situ simultaneous determination of trace elements, U–Pb and Lu–Hf isotopes in zircon and baddeleyite. Chinese Science Bulletin 53, 1565–1573.
Xing, F.M., Xu, X., 1994. Two A-type syenite–granite belts in Anhui. Chinese Journal of geochemistry 13, 340–354.
Xiong, X.L., Adam, J., Green, T.H., 2005. Rutile stability and rutile/melt HFSE partitioning during partial melting of hydrous basalt: implications for TTG genesis. Chemical Geology 218, 339–359.
Xu, G.Z., Zhou, R., Yan, Z., Yu, H.Q., Wang, Y.F., Yang, M.S., Li, B., 2001. Discussion on the evidences of Mesozoic lithosphere thinning and its dynamic mechanism in Jiaodong area. Geotectonica et Metallogenia 25, 368–380 (in Chinese with English abstract).
Xu, Y.G., Huang, X.L., Ma, J.L., Wang, Y.B., Iizuka, Y., Xu, J.F., Wang, Q., Wu, X.Y., 2004a. Crust–mantle interaction during thetectono-thermal reactivation of the North China Craton: constraints from SHRIMP zircon U–Pb chronology and geochemistry of Mesozoic plutons from western Shandong. Contributions to Mineralogy and Petrology 147, 750–767.
Xu, Y.G., Ma, J.L., Huang, X.L., Iizuka, Y., Chung, S.L., Wang, Y.B., Wu, X.Y., 2004b. Early Cretaceous gabbroic complex from Yinan, Shandong Province: petrogenesis and mantle domains beneath the North China Craton. International Journal of Earth Sciences 93, 1025–1041.
Xu, H.J., Ma, C.Q., Ye, K., 2007. Early cretaceous granitoids and their implications for the collapse of the Dabie orogen, eastern China: SHRIMP zircon U–Pb dating and geochemistry. Chemical Geology 240, 238–259.
Xu, Y.G., Li, H.Y., Pang, C.J., He, B., 2009. On the timing and duration of the destruction of the North China Craton. Chinese Science Bulletin 54, 3379–3396.
Xue, H.M., Liu, F.L., Meng, F.C., 2006a. Petrogenesis of Neoproterozoic granitoids from the Wulian region in the Sulu orogen: Sr–Nd isotopic constraints. Earth Science-Journal of China University of Geosciences 31, 497–504 (in Chinese with English abstract).
Xue, H.M., Liu, F.L., Meng, F.C., 2006b. Major and trace element geochemistry of granitic gneisses from Sulu orogen, eastern Shandong Peninsula: evidence for a Neoproterozoic active continental margin in the northern margin of the Yangtze craton. Acta Petrologica Sinica 22, 1779–1790 (in Chinese with English abstract).
Yan, J., Zhang, X., Chen, J.F., Zhao, H.L., 2001. Sr, Nd isotopic characteristics of the Jinan gabbro intrusion. Bulletin of Mineralogy, Petrology and Geochemistry 20, 302–305 (in Chinese with English abstract).
Yan, J., Chen, J.F., Yu, G., Qian, H., Zhou, T.X., 2003. Pb isotopic characteristics of Late Mesozoic mafic rocks from the Lower Yangtze region: evidence for enriched mantle. Geological Journal China University 9, 195–206 (in Chinese with English abstract).
Yan, J., Chen, J.F., Xie, Z., Yang, G., Yu, G., Qian, H., 2005. Geochemistry of Late Mesozoic basalts from Kedoushan in the middle and lower Yangtze regions: constraints on characteristics and evolution of the lithospheric mantle. Geochimica 34, 455–469 (in Chinese with English abstract).
Yan, G.H., Cai, J.H., Ren, K.X., Mu, B.L., Li, F.T., Chu, Z.Y., 2008. Nd, Sr and Pb isotopic geochemistry of late-Mesozoic alkaline-rich intrusions from the Tanlu Fault zone: evidence of the magma source. Acta Petrologica Sinica 24, 1223–1236 (in Chinese with English abstract).
Yang, C.H., 2007. Chronology and geochemistry of Mesozoic high-Mg diorites in Western Shandong: constraints on lithospheric evolution of the North China Craton. Ph.D. thesis, Jilin University (in Chinese with English abstract).
Yang, J.H., Chung, S.L., Zhai, M.G., Zhou, X.H., 2004. Geochemical and Sr–Nd–Pb isotopic compositions of mafic dikes from the Jiaodong Peninsula, China: evidence for vein-plus-peridotite melting in the lithospheric mantle. Lithos 73, 145–160.
Yang, C.H., Xu, W.L., Yang, D.B., Liu, C.C., Liu, X.M., Hu, Z.C., 2005a. Petrogenesis of Mesozoic high-Mg diorites in western Shandong: evidence from chronology and petro-geochemistry. Journal of China University of Geosciences 16, 297–308.
Yang, J.H., Chung, S.L., Wilde, S.A., Wu, F.Y., Chu, M.F., Lo, C.H., Fan, H.R., 2005b. Petrogenesis of post-orogenic syenites in the Sulu Orogenic Belt, East China: geochronological, geochemical and Nd–Sr isotopic evidence. Chemical Geology 214, 99–125.
Yang, J.H., Wu, F.Y., Chung, S.L., Wilde, S.A., Chu, M.F., Lo, C.H., Song, B., 2005c. Petrogenesis of Early Cretaceous intrusions in the Sulu ultrahigh-pressure orogenic belt, east China and their relationship to lithospheric thinning. Chemical Geology 222, 200–231.
Yang, J.H., Wu, F.Y., Chung, S.L., Wilde, S.A., Chu, M.F., 2006. A hybrid origin for the Qianshan A-type granite, northeast China: geochemical and Sr–Nd–Hf isotopic evidence. Lithos 89, 89–106.
Yang, J.H., Wu, F.Y., Xie, L.W., Liu, X.M., 2007. Petrogenesis and tectonic implications of Kuangdonggou syenites in the Liaodong Peninsula, east North China Craton: constraints from in-situ zircon U–Pb ages and Hf isotopes. Acta Petrologica Sinica 23, 263–276 (in Chinese with English abstract).
Ying, J.F., Zhou, X.H., Zhang, H.F., 2004. Geochemical and isotopic investigation of the Laiwu–Zibo carbonatites from western Shandong Province, China and implications for their petrogenesis and enriched mantle source. Lithos 75, 413–426.
Ying, J.F., Zhang, H.F., Sun, M., Tang, Y.J., Zhou, X.H., Liu, X.M., 2007. Petrology and geochemistry of Zijinshan alkaline intrusive complex in Shanxi Province, western North China Craton: implication for magma mixing of different sources in an extensional regime. Lithos 98, 45–66.
Zeng, L.S., Liang, F.H., Asimow, P., Chen, F.Y., Chen, J., 2009. Partial melting of deeply subducted continental crust and the formation of quartzo-feldspathic polyphase inclusions in the Sulu UHP eclogites. Chinese Science Bulletin 54, 2580–2594.
Zhang, H.F., Sun, M., Zhou, X.H., Fan, W.M., Zhai, M.G., Yin, J.F., 2002. Mesozoic lithosphere destruction beneath the North China Craton: evidence from major-, trace-element and Sr–Nd–Pb isotope studies of Fangcheng basalts. Contributions to Mineralogy and Petrology 144, 241–253.
Zhang, H.F., Sun, M., Zhou, X.H., Fan, W.M., Zheng, J.P., 2003. Secular evolution of the lithosphere beneath the eastern North China Craton: evidence from Mesozoic basalts and high-Mg andesites. Geochimica et Cosmochimica Acta 67, 4373–4387.
Zhang, H.F., Zhai, M.G., He, Z.F., Peng, P., Xu, B.L., 2004. Petrogenesis and implications of the sodium-rich granites from the Kunyushan complex, eastern Shandong province. Acta Petrologica Sinica 20, 369–380 (in Chinese with English abstract).
Zhang, H.F., Sun, M., Zhou, X.H., Ying, J.F., 2005a. Geochemical constraints on the origin of Mesozoic alkaline intrusive complexes from the North China Craton and tectonic implications. Lithos 81, 297–317.
Zhang, H.F., Zhou, X.H., Fan, W.M., Sun, M., Guo, F., Ying, J.F., Tang, Y.J., Zhang, J., Niu, L.F., 2005b. Nature, composition, enrichment processes and its mechanism of the Mesozoic lithospheric mantle beneath the southeastern North China Craton. Acta Petrologica Sinica 21, 1271–1280 (in Chinese with English abstract).
Zhang, Q., Li, C.D., Wang, Y., Wang, Y.L., Jin, W.J., Jia, X.Q., 2005c. Mesozoic high-Sr and Low-Yb granitoids and low-Sr and high-Yb granitoids in eastern China: comparison and geological implications. Acta Petrologica Sinica 21, 1527–1537 (in Chinese with English abstract).
Zhang, Q., Wang, Y., Li, C.D., Jin, W.J., Jia, X.Q., 2006. A granite classification based on pressures. Geological Bulletin of China 25, 1274–1278 (in Chinese with English abstract).
Zhang, Q., Wang, Y., Xiong, X.L., Li, C.D., 2008. Adakite and Granite: Challenge and Opportunity. China Land Press, Beijing, pp. 1–340 (in Chinese with English summary).

Zhang, Q., Jin, W.J., Li, C.D., Wang, Y.L., 2009a. Yanshanian large-scale magmatism and lithosphere thinning in Eastern China: relation to large igneous province. Earth Science Frontiers 16, 21–51 (in Chinese with English abstract).
Zhang, R.Y., Liou, J.G., Ernst, W.G., 2009b. The Dabie–Sulu continental collision zone: a comprehensive review. Gondwana Research 16, 1–26.
Zhao, G.T., Wang, W.Z., 1998. Compositional variation and its significance of amphiboles from Laoshan granitods. Journal of Ocean University of Qingdao 28, 609–614 (in Chinese with English abstract).
Zhao, Z.F., Zheng, Y.F., 2009. Remelting of subducted continental lithosphere: petrogenesis of Mesozoic magmatic rocks in the Dabie–Sulu orogenic belt. Science in China Series D: Earth Sciences 52, 1295–1318.
Zhao, J.X., Shiraishi, K., Ellis, D.J., Sheraton, J.W., 1995. Geochemical and isotopic studies of syenites from the Yamoto Mountains, East Antartica: implication for the origin of syenitic magmas. Geochimica et Cosmochimica Acta 59, 1363–1385.
Zhao, G.T., Wang, D.Z., Cao, Q.C., 1997. The geochemistry and genesis of the Laoshan granitoids, Sandong Province. Geological Journal of China Universities 3, 1–15.
Zhao, Z.F., Zheng, Y.F., Wei, C.S., Wu, Y.B., 2007. Post-collisional granitoids from the Dabie orogen in China: zircon U–Pb age, element and O isotope evidence for recycling of subducted continental crust. Lithos 93, 248–272.
Zheng, Y.F., 2008. A perspective view on ultrahigh-pressure metamorphism and continental collision in the Dabie–Sulu orogenic belt. Chinese Science Bulletin 53, 3081–3104.
Zhou, J.B., Zheng, Y.F., Wu, Y.B., 2003a. Zircon U–Pb ages for Wulian granites in northwest Sulu and their tectonic implications. Chinese Science Bulletin 48, 379–384.
Zhou, J.B., Zheng, Y.F., Zhao, Z.F., 2003b. Zircon U–Pb dating on Mesozoic granitoids at Wulian, Shangdong Province. Geological Journal of China Universities 9, 185–194 (in Chinese with English abstract).
Zindler, A., Hart, S.R., 1986. Chemical geodynamics. Annual Review of Earth Planetary Sciences 14, 493–571.
Zorin, Y.A., 1999. Geodynamics of the western part of the Mongolia–Okhotsk collisional belt, Trans-Baikal region (Russia) and Mongolia. Tectonophysics 306, 33–56.
Zou, H.B., Zindler, A., Xu, X.S., Qi, Q., 2000. Major, trace element, and Nd, Sr and Pb isotope studies of Cenozoic basalts in SE China: mantle sources, regional variations, and tectonic significance. Chemical Geology 171, 33–47.